12-19-2003

Electrospray Fundamentals and Non-Covalent Peptide-Lipid Interactions as Studied by Fourier Transform Ion Cyclotron Reonance Mass Spectrometry

Yan Li
University of New Orleans

ELECTROSPRAY FUNDAMENTALS AND NON-COVALENT PEPTIDE-LIPID INTERACTIONS AS STUDIED BY FOURIER TRANSFORM ION CYCLOTRON RESONANCE MASS SPECTROMETRY

A Dissertation

Submitted to the Graduate Faculty of the
University of New Orleans
in partial fulfillment of the
requirements for the degree of

Doctor of Philosophy
in
The Department of Chemistry

by

Yan Li

B.S., Nankai University, 1991
M.S., Nankai University, 1994

December 2003

ACKNOWLEDGEMENTS

First of all, my thanks go to my parents and all the great teachers that I had throughout my life. They guided me to love this world and to try my best to contribute to a better future.

I am very grateful to the Department of Chemistry and the Graduate School of the University of New Orleans for offering me the great chance to study and work at this great place.

I am full of appreciation to my supervisor, Dr Richard B. Cole. During the four-year research, I learned a lot from him. Two of my projects stalled at the very beginning. I struggled for a long time, but made little progress. He always helped me and encouraged me to hang in there. Because of that, we finally found hope from despair.

I would like to thank my committee members, Dr. Ronald F. Evilia, Dr. Matthew Tarr, Dr. John B. Wiley, and Dr. Zeev Rosenzweig. They spent time reading my reports. They asked enlightening questions during my general exam. They offered helpful suggestions whenever I came to them. To me, their support is a memory too warm to forget.

I also would like to thank my other coworkers: Dr. Heitz, Dr. Le Grimellec and especially Dr. Boguslaw P. Pozniak for their big help.

My endless appreciation goes to my husband, Mr. Jiangpeng Shi, for his unlimited support.

TABLE OF CONTENTS

ABSTRACT

A novel electrochemical probe has been designed, built, and used to characterize the distribution in solution potential within the metal capillary and Taylor cone of the electrospray (ES) device. Results show that the measured potential difference increases as the internal probe travels toward the ES capillary exit, with values rising sharply as the base of the Taylor cone is penetrated. Higher conductivity solutions exhibit potentials of higher magnitude at longer distances away from the counter electrode, but these same solutions show lower potentials near the ES capillary exit. Removal of easily oxidizable species from the solution causes the measured potential difference to have nonzero values at distances further within the capillary, and the values measured at all points are raised. The influence of the diameter of the spray tip employed for nano-electrospray mass spectrometry (nano-ES-MS) upon mass spectral charge state distributions was investigated. A detailed comparison of charge state distributions obtained for nanospray capillaries of varying diameters was undertaken while systematically varying experimental parameters such as sample flow rate, analyte concentration, solvent composition, and electrospray current. The general tendency to obtain higher charge states from narrow diameter capillaries was conserved throughout, but tips with smaller orifices were more sensitive to sample flow rate, while tips with larger orifices were more sensitive to analyte concentration and pH of the solution.

Electrospray mass spectrometry (ES-MS) has been employed to study noncovalent associations between lipids and fusion peptides. Detailed binding specificities between selected phospholipids and model fusion peptides were investigated. Strong evidence has been compiled to demonstrate the importance of the initial hydrophobic interaction to the observation of lipid-peptide binding by ES-MS. Initial hydrophobic interactions in solution contributed heavily to the formation of these peptide-lipid complexes, particularly for [peptide+PC] complexes, whereas electrostatic interactions played a larger role for [peptide+PG] complexes. The influence of solution pH and degree of unsaturation of lipids upon the binding strength of [peptide+PC] complexes were also investigated. These experiments help to establish ES-MS as a viable new biotechnology tool capable of providing valuable information regarding the strength of hydrophobically driven, noncovalent interactions.

INTRODUCTION

The phenomenon of electrospray (ES), i.e., the dispersion of liquid into small droplets by an electrostatic field, was studied many years ago [1]. After the ES source was successfully coupled with mass spectrometry, ES-MS has proven to be an extremely powerful tool which makes it possible to study a wide variety of samples including biological macromolecules and other nonvolatile compounds, many of which are not readily amenable to analysis by other methods[2-5]. Along with its steadily increasing applications, many fundamental studies have focused on the individual steps that are responsible for transforming analytes in solution into gas-phase ions [6-25].

It is well-known that in the positive ion mode, the imposed high electric field used in ES induces an enrichment of positive ions at the surface of the solution at the ES capillary exit, and tends to pull the liquid containing an excess of positive charge toward the counter electrode. The surface tension of the solution exerts a pull in the opposite direction. The net outcome is that the solution forms a "Taylor cone" at the ES capillary exit to balance these opposing effects. If the applied field is sufficiently high, a fine, charged filament emerges from the cone tip and the high charge density on this "jet" causes the break-up of the liquid into small charged droplets. Solvent evaporation reduces the volume of the droplet at constant charge, causing fission of the droplets into smaller droplets and, after one or more fission events, gas-phase ions are formed.

It is evident that electrochemical phenomena play a vital role in creating and sustaining charged droplet formation at the Taylor cone[26]. However, it is not clear how the local electric field varies within the solution emerging from a metal capillary held at high potential. The ability to characterize these variations in potential is important for the detailed understanding of the functioning of the ES device, and in particular, the redox reactions that occur within the electrospray emitter. To our knowledge, the only reported work in this area is a calculated potential distribution within a cone consisting of pure methanol by Kebarle and coworkers[27] that used the simplifying assumption that there were no charge carriers present, and a more detailed computational simulation done by Van Berkel and coworkers at Oak Ridge National Laboratory[28]). The latter report concluded that the majority of the current from the redox reaction is generated within a 200-300 um region near the spray exit. Metal-solution interface potentials within the spray capillary were also calculated. Our goal is to experimentally measure the potential distribution and map the potential gradients within the electrospray capillary and Taylor cone. If one seeks to gain control of the electrochemical environment inside the ES device, it is necessary to apply fundamental electrochemical concepts to interpret potential distributions within the electrospray capillary.

One distinguishing characteristic of electrospray mass spectrometry (ES-MS) is the propensity to form and detect multiply charged analyte species which enables observation of macromolecules at relatively low m/z values[29-31]. Not only does the ES process make the detection of large biomolecules possible, but in addition, the charge state distribution of the analyte can serve as a probe to monitor its conformational dynamics[32-36]. Several models have been built to depict the details of the ionization process in ES-MS[36-41], and a

better understanding of the factors that influence the analyte charge state distribution can help to clarify mechanistic aspects of the ES process. It has been shown that the analyte structure/conformation[33-35,42,43], analyte concentration[36,40,44,46], gas-phase reactivity[47-55], solution pH[32,53,56-60], solvent composition[61-63], and ES instrumental parameters[48,50,64,65], all have influences on the final charge state distribution observed in ES-MS.

More recently developed nano-electrospray (nano-ES) is different from conventional electrospray (the latter typically employs 4-200 microliter/min flow rates through 0.1 mm diameter capillaries) in that the employed nanospray tips have very small orifices, usually less than 10 µm in diameter[66], and flow rates are in the 10-500 nL/min range. Compared to conventional ES, there are several advantages that make nano-ES very attractive: 1) the onset of ES occurs at a lower applied voltage which helps to reduce the problem of electrical (corona) discharge; 2) because the sample flow rate is so low, much less sample is consumed; 3) the radii of initially produced droplets are smaller so the ionization efficiency is higher; 4) nebulizing gas and drying gas are not necessary, so ion transmission is higher[66]. Furthermore, it is believed that the low solvent flow rate affects the mechanism of ion formation. Mann et al.[67] theoretically described the electrostatic dispersion in nano-ES. Karas et al.[68] presented a model to explain the origin of the different mass spectral characteristics of ionspray and nanospray by suggesting different "predominant fission pathways" depending on the size of the initial droplets. They point out that ions with low surface activities experience greater losses to the residue during fission events while the more surface active species become enriched. In nanospray, because ions are desorbed from smaller initial droplets that presumably undergo fewer fission events, Karas and coworkers[69] reasoned that analytes with lower surface activities

(e.g., oligosaccharides, glycosides and glycoproteins) would experience higher transmission through the ion source, as compared to conventional electrospray.

Nanospray emitters also exhibit certain drawbacks such as fragility, causing a high propensity to fracture the sharp end of the tip. This is because, unlike the emitter used in conventional ES that is typically made of stainless steel, nanotips are usually made of glass that is coated with a conductive metal. Also contributing to the short lifetimes of nanotips are the problems of corrosion of the conductive coating, and sample clogging[70]. Another issue is that, owing to manufacturing difficulties, the orifice of the nanotip is less uniform than in conventional ES.

The ability to obtain reproducible charge state distributions can have an enormous impact on the accuracy of studies that rely on a single charge state for quantification. In addition, MS/MS studies performed on multiply charged precursors require a minimum signal for the selected precursor ion. The success of such tandem mass spectrometry experiments can hinge on the ability of the analyst to control conditions to favor the production of ions of specified charge states. For a given precursor molecule, ions of higher charge state are known to undergo decompositions more readily than those of lower charge state[68,69,71,72]. Moreover, because attempts have been made to use nano-ES-MS to probe the binding and conformational properties of noncovalent complexes[73], the exact nature of interactions may change as the charge state shifts. For these reasons, it is important to obtain a detailed understanding of the effects of the physical characteristics of the nanospray tip on the charge state distributions of analytes.

Fourier Transform Ion Cyclotron Resonance Mass Spectrometry (FT-ICR MS) has been widely practiced since its inception in 1974[74], because of its ability to reach higher

resolution and accuracy than other mass spectrometer. When coupled with electrospray ionization (ESI)[75,76] or matrix-assisted laser desorption ionization (MALDI)[77,78], it becomes a very powerful technique for study of macro-biomolecules. Electrospray, especially nano-electrospray, known as a soft ionization process, makes it possible for the noncovalent complexes formed in the solution to transfer into the gas phase. Nano-ES-FTMS has become a novel tool for studying of various protein-ligand noncovalent interactions[79-82].

The fusion of a viral membrane with the host cell membrane is critical to infection by viruses such as HIV and influenza. This membrane fusion process is facilitated by viral envelope glycoproteins called fusion proteins. Trying to interrupt viral membrane fusion became a new disease therapy[83], which requires a detailed knowledge of the fusion mechanism. Fusion peptides correspond to short regions, rich in hydrophobic residues, within the ectodomain of these proteins, which can initiate membrane fusion by leading insertion into the host cell membrane[83-85]. It is believed that fusion peptides not only exist in all viral fusion proteins, they also are a central motif in the mechanism of fusion[86]. Investigation of interactions between fusion peptides and lipid bilayers is essential for improving the understanding of membrane fusion process. In addition, when associated with a polar nuclear localization sequence, thus offering amphipathic character, fusion peptides can act as efficient drug carriers by facilitating drug insertion and translocation across the cellular membrane[87].

It has been shown by a variety of methods such as CD, FTIR, NMR[88-92] that hydrophobic interactions, electrostatic interactions and conformational changes of both the peptide and the membrane all contribute to the transfer of the peptide from the aqueous phase through

the lipid membrane[93-96]. However, reports of the use of mass spectrometry to observe noncovalent complexes between lipids and proteins (soluble[97] or membrane[98]) or peptide[our paper] have appeared only very recently.

Electrospray mass spectrometry (ES-MS) has the advantage of preserving the non-covalent associations that exist in solution into the gas phase. However, it always concerned that gas-phase noncovalent adduct ions observed by mass spectrometry may not reflect the status of the component molecules in solution[99-103]. Up until now, a moderate noncovalent binding strength was considered to be essential to allowing observation of intact complexes, and it has been established that upon transfer to the gas-phase, electrostatic interactions are strengthened, while hydrophobic interactions are weakened[104].

Noncovalent lipid-peptide or lipid-protein interactions are characterized by both electrostatic and hydrophobic components. Our goal is to specifically probe the hydrophobic aspect of initial binding, and we target lipid interactions with peptides.We also would like to further investigate the detailed binding specificities between the selected phospholipids and model fusion peptides.

CHAPTER 1

Mapping of Potential Gradients within the Electrospray Emitter

Yan Li, Boguslaw P. Pozniak, Richard B. Cole*

Department of Chemistry, University of New Orleans,
2000 Lakeshore Dr., New Orleans, LA 70148

Abstract

A novel electrochemical probe has been designed, built, and used to characterize the distribution in solution potential within the metal capillary and Taylor cone of the electrospray (ES) device. The measurement system consists of three electrodes – a counter electrode held at highly negative potential that serves as the cathode, and two anodes consisting of a disk-shaped, mobile, internal (working) electrode, and the internal surface of the surrounding ES capillary (auxiliary electrode, held at ground potential). One-dimensional Differential Electrospray Emitter Potential (DEEP) maps detailing solution potential gradients within the electrospray emitter and in the region of the Taylor cone are constructed by measuring the potential at the working electrode vs. the ES capillary, as a function of working electrode position along the ES capillary axis. Results show that the measured potential difference increases as the internal probe travels toward the ES capillary exit, with values rising sharply as the base of the Taylor cone is penetrated. Higher conductivity solutions exhibit potentials of higher magnitude at longer distances away from the counter electrode, but these same solutions show lower potentials near the ES capillary exit. Removal of easily oxidizable species from the solution causes the measured potential difference to have nonzero values at distances further within the capillary, and the values measured at all points are raised. Results are consistent with the characterization of the electrospray system as a controlled-current electrolytic flow cell. Elucidation of the electrochemical details of the electrospray process can lead to mass spectrometric signal enhancement of certain species present in

the spraying liquid, and also allow the detection of molecules that are usually not observable due to their low ionization efficiencies.

*Author to whom correspondence should be addressed

Introduction

The phenomenon of electrospray (ES), i.e., the dispersion of liquid into small droplets by an electrostatic field, was studied many years ago[1]. After the ES source was successfully coupled with mass spectrometry, ES-MS has proven to be an extremely powerful tool which makes it possible to study a wide variety of samples including biological macromolecules and other nonvolatile compounds, many of which are not readily amenable to analysis by other methods[2-5]. Along with its steadily increasing applications, many fundamental studies have focused on the individual steps that are responsible for transforming analytes in solution into gas-phase ions[6-24].

It is well-known that in the positive ion mode, the imposed high electric field used in ES induces an enrichment of positive ions at the surface of the solution at the ES capillary exit, and tends to pull the liquid containing an excess of positive charge toward the counter electrode. The surface tension of the solution exerts a pull in the opposite direction. The net outcome is that the solution forms a "Taylor cone" at the ES capillary exit to balance these opposing effects. If the applied field is sufficiently high, a fine, charged filament emerges from the cone tip and the high charge density on this "jet" causes the break-up of the liquid into small charged droplets. Solvent evaporation reduces the volume of the droplet at constant charge, causing fission of the droplets into smaller droplets and, after one or more fission events, gas-phase ions are formed.

It is evident that electrochemical phenomena play a vital role in creating and sustaining charged droplet formation at the Taylor cone[26]. However, it is not clear how the local electric field varies within the solution emerging from a metal capillary held at high potential. The ability to characterize these variations in potential is important for the detailed understanding of the functioning of the ES device, and in particular, the redox reactions that occur within the electrospray emitter. To our knowledge, the only reported work in this area is a calculated potential distribution within a cone consisting of pure methanol by Kebarle and coworkers[27] that used the simplifying assumption that there were no charge carriers present, and a more detailed computational simulation done by Van Berkel and coworkers at Oak Ridge National Laboratory[28]. The latter report concluded that the majority of the current from the redox reaction is generated within a 200-300 um region near the spray exit. Metal-solution interface potentials within the spray capillary were also calculated. The goal of the current report is to experimentally measure the potential distribution and map the potential gradients within the electrospray capillary and Taylor cone. If one seeks to gain control of the electrochemical environment inside the ES device, it is necessary to apply fundamental electrochemical concepts to interpret potential distributions within the electrospray capillary.

Experimental Section

Chemicals

HPLC-grade acetonitrile, water, methanol, and lithium trifluoromethanesulfonate ($LiCF_3SO_3$) were purchased from EM science (Gibbstown, NJ); acetonitrile was further

purified by distillation followed by introduction of phosphorus pentoxide (P_2O_5) powder to remove traces of water.

Hardware Configuration

A 660A electrochemical workstation (CH Instruments, Austin, TX) was used as the electronic detector. To protect the electronic detector from the potential damage of high voltage arcing, for all positive ion mode work in this study, a high (negative) voltage was applied to the counter electrode while keeping the auxiliary electrode grounded. Because all potential measurements at the internal (working) electrode were made relative to the ES capillary (auxiliary electrode), displayed Differential Electrospray Emitter Potential (DEEP) maps depicting this *difference* in potential as a function of working electrode movement are expected to be similar to those that would be obtained for alternative positive mode electrospray configurations where the ES capillary (anode) is floated at a fixed high voltage and the counter electrode (cathode) is maintained near ground.

Electrospray Conditions

The distance between the counter electrode and the ES spray capillary was fixed at 6.0 mm. The flow rate adopted in this study was 200 µl/hr, unless otherwise noted. The high voltage applied to the counter electrode was adjusted to give the most stable spray conditions: values ranged from 3 kV to 4 kV, and exact values are noted in the text and figures. All comparative studies shown in a single figure panel were performed using the same working electrode.

Data Treatment

For all generated figures, at each point, at least three measurements were made. Error bars represent one standard deviation (1s) of the measured values. For certain solutions, it was noted that measured potentials would unexpectedly achieve low positive values when the working electrode was located far within the ES capillary. While never large (always <200 mV), the magnitude of this phenomenon was highly dependent on the solvent used, and the particular employed platinum working electrode. When present, the slightly positive values were observed to persist even after the high voltage was shut off. These near-zero relative potential values, considered to arise from slight differences in the polycrystalline surfaces of the Pt electrodes and peculiarities of the histories of the individual electrodes, were measured in a point-by-point fashion with the solvent flowing and the high voltage off. The minor "baseline" potentials obtained in this way were subtracted from the data shown in Figures 2, 3b, and 5. In other figures, no corrections were made.

Results and Discussion

Measurement Device. A unique electrochemical cell that places a working electrode inside the electrospray capillary was described[105] and used to study redox reaction products of polycyclic aromatic hydrocarbons (PAHs), and other aromatic compounds[106]. A distinguishing feature of the design of this electrochemical cell is that the working electrode is shielded from the sample solution until reaching the region near the capillary exit. We would like to exploit a modified version of this device in a way that it has never been used before, i.e., to use the internal electrode to measure potential gradients along

the central axis of the ES capillary, and even within the Taylor cone. These data can be used to construct one-dimensional Differential Electrospray Emitter Potential (DEEP) maps revealing the potential profile within the emitter, as a function of distance along its axis.

Figure 1 schematically shows the DEEP mapping device that was constructed in-house. The counter electrode (A) is a 0.9 inch thick brass plate that was held at high (negative) voltage during all experiments. The ES spray capillary (C) serves as the auxiliary electrode. It consists of a platinum (99.95%) cylinder with 0.5 mm i.d., 0.6 mm o.d., (Goodfellow Cambridge Limited, Cambridge, UK), that was held at ground (earth) potential during all experiments. The working electrode (B) is a platinum wire (99.9%, 0.127 mm diameter) (Alfa Aesar, MA) sealed (with epoxy-resin) inside a fused silica tube (220 µm i.d., 320 µm o.d.) (SGE Incorporated, TX) such that only the very end of the wire (virtually a disk) is exposed to the solution. The fused silica layer thus prevents contact with the solution until the liquid reaches the working electrode surface near the ES capillary exit. A position controller (E) was built to move the working electrode independently with respect to the outer (ES) capillary. The minimum division of the controller is 20 µm which corresponds to the minimum distance that the working electrode can be moved reliably. The x-axis zero point of all obtained DEEP maps corresponds to the position where the working electrode surface is flush with the ES capillary exit. Negative position values correspond to working electrode placement within the capillary, while positive values indicate that the working electrode is protruding out of the capillary into the Taylor cone. The syringe for sample delivery was mounted on a Cole-Parmer 74900 series syringe pump (Vernon Hills, IL). The high

voltage was supplied by a Glassman (High Bridge, NJ) high voltage power supply. The platinum wire constituting the working electrode penetrates through a cross union (F) (Upchurch Scientific, Oak Harbor, WA) to provide electrical contact to the power supply. The sample solution is introduced into the cross union and it passes through the annulus between the outer wall of the fused silica tube (shielding the working electrode), and the inner wall of the platinum auxiliary electrode (ES capillary). In addition to preventing the solution from making contact with the working electrode during transport to the spray tip, the fused silica also prevents direct electrical contact between the auxiliary and working electrodes. Moreover, it offers the platinum wire necessary firmness to enable mounting on the position controller. By properly adjusting the tightness between the cross union and working electrode, one can move the working electrode back and forth without causing the solution to leak. In our experiments, nebulizing gas was not employed; this helped to keep the potential gradients as unperturbed as possible.

The above two-electrode system was employed in all experiments. The open circuit potential of the exposed platinum wire tip (working electrode) was measured with respect to the potential of the ES capillary (auxiliary electrode). This potential difference varies with position of the working electrode wire tip. In the actual instrumental wiring, the ES capillary was grounded, thereby giving it a constant potential over the course of an experiment, and it was hard-wired to the working electrode outlet of the potentiostat. The reference electrode port of the potentiostat was shorted to the counter electrode port, and they both were connected to the platinum wire probe. Owing to this arrangement, positive potentials read by the instrument mean negative potentials at the exposed platinum wire. For electrospray operation in the positive mode, set up such that the spray capillary is

grounded and the counter electrode is at high negative potential, the wire-probe in the emerging solution will have potentials lower than the surrounding capillary. Because potential is a value relative to a chosen reference zero point, the DEEP maps are made with the y-axis showing increasingly negative values of potential relative to the grounded ES capillary (auxiliary electrode). When the working electrode is located at points within the ES capillary (negative x-axis values on obtained maps), the measured potentials are reflective of, but of lower magnitude than, the potentials at the metal-solution interface at that distance along the external capillary.

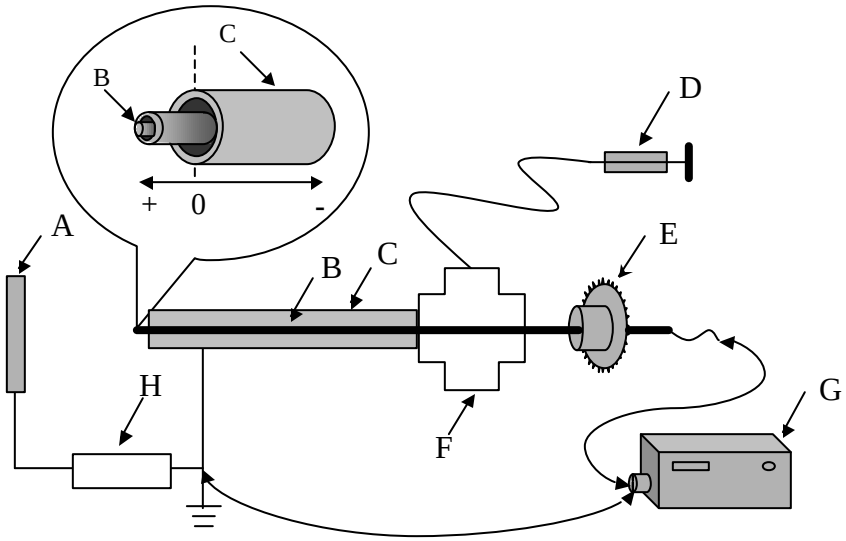

Fig. 1. Schematic diagram of the device employed to construct one-dimensional Differential Electrospray Emitter Potential (DEEP) maps. A: counter electrode; B: working electrode sealed in fused silica tube; C: ES capillary, also the auxiliary electrode; D: syringe pump; E: working electrode position controller; F: cross union; G: electrochemical work station; H: high voltage supply. The inset shows a blow up of the working electrode assembly sealed in a fused silica tube (B, sealant not shown) surrounded by the ES capillary. The surface of the working electrode that comes in contact with the sample solution is thus disk-like in shape and coplanar with the ES capillary exit aperture.

Generation of DEEP Maps Showing Potential Gradients. When the electrospray high voltage is switched on, the potential difference that is being measured between the ES capillary and the internal wire probe is initially rising rapidly. While the time required to achieve a stable electrospray and resulting steady ES current is quite short, the time needed to achieve a stable relative potential reading can be significantly longer. The exact delay varies with the solvent system from a few seconds for the methanol/water system, to minutes for acetonitrile or the acetonitrile/water system. With no faradaic current flow, the electrode potential is determined by the presence of electrochemically-active species in the vicinity of the electrode surface, and ions need time to migrate to establish steady state concentration gradients. Flow of the solution in our ES capillary has a linear velocity of about 0.5 mm per second. Liquid in the electrode region is being refreshed continuously, and it takes less than one second to replenish the volume of the Taylor cone. Importantly, because the sprayed liquid has changed somewhat in composition as compared to the liquid arriving into the capillary owing to oxidation reactions occurring on the capillary walls near the capillary exit[28,107], and possible ensuing solution reactions, concentration gradients must become established in opposition to the flow direction. For this reason, the time to reach a steady state could be significantly prolonged as compared to the same system in quiescent solution.

It was also noted that when the position of the wire probe was moved, causing a fluctuation in measured potential, it took at least a short time for the potential reading to stabilize, even after only a small distance (e.g. 40 μm) of electrode movement. Moreover, it was noted that the time required to reach stability was prolonged for movement between points deeper inside the capillary as compared to points closer to the capillary

tip. We attribute the slow equilibration time principally to the change in the chemical composition of the liquid in response to the consumption and production of electroactive species that undergo diffusion and migration, including movement in the upstream direction. The exact time required for equilibration will depend upon the solvent selected, the flow rate employed, and the volume of the emitter. Delay times observed by Van Berkel[108], in his system were of the order of 5-7 minutes, which is in agreement with our observations at close ranges, but at very negative "x-positions" where the travel distance upstream to the working electrode was furthest, the time required for potentials to equilibrate was often significantly longer.

Potential Gradient In 1:1 Methanol/Water. 50/50 v/v methanol/water is perhaps the most popular solvent for ES and it is widely used for analyses of peptides and proteins. Because of the widespread use of this solvent system, we chose it to begin our experiments to map the variations in potential along the ES emitter axis. It was quickly surmised that in order to achieve reproducible one-dimensional maps of potential variations, it was extremely critical to establish ES operating conditions that allowed Taylor cone stability for prolonged time periods (e.g., up to 30 min). This long term stability was most readily achieved under conditions where the emitter was operating in the so-called "cone-jet" mode with a straight or curved generatrix[109]. It was found that in other operational modes, such as the "pulsed cone-jet" or "multicone-jet" modes, where the Taylor cone shape may be periodically changing, discontinuities in obtained maps were observed to occur at points where the cone had undergone reshaping. At these instances the "jumps" in measured potential were sudden, irregular, and did not

necessarily finish with an eventual return to the prior value. For this reason, all data was acquired under conditions of "cone-jet" emission.

For 1:1 (v:v) methanol:water, used without added supporting electrolyte, a stable electrospray was achieved with a flow rate of 200 µl/hr and HV = 4000 V. Figure 2 displays obtained one-dimensional DEEP maps showing the total range (2a), and near range (2b) of the variations in measured potential as a function of working electrode position. The zero position on the x-axis corresponds to the situation where the face of the electrode (wire) is aligned exactly with the exit of the electrospray capillary. It can be seen that within the Taylor cone (positive values on the x-axis), the potential is most oxidative and the gradient (derivative of the potential) is steepest. In moving away from the Taylor cone, the gradient decreases as the electrode (wire probe) is pulled into the capillary (negative values on the x-axis), and becomes virtually flat at about 2000 µm away from the exit.

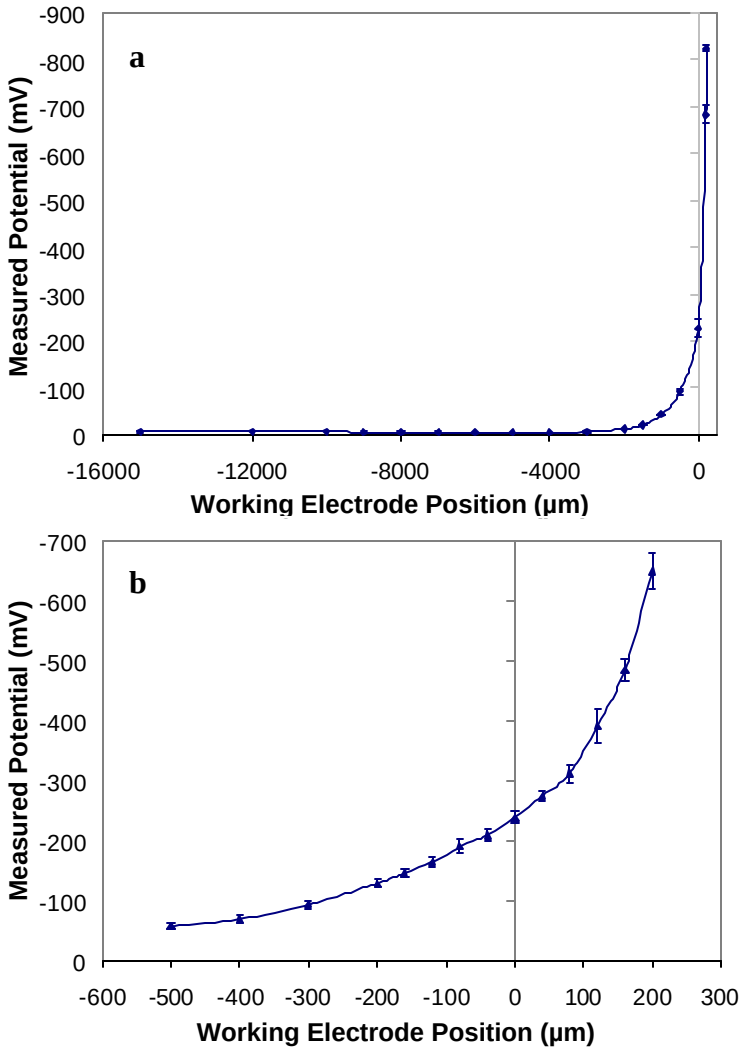

Fig. 2. One-dimensional DEEP maps (measured open-circuit potential difference vs working electrode placement) from water:methanol (1:1) solution over: (a) the total range , (b) the range nearest to the ES capillary exit; . HV = 4000 Volts, V_f = 200 ul/hr.

In open circuit potential measurements such as those undertaken to generate Figure 2, the potential of one electrode is recorded with respect to another electrode. There is additional drop of potential between the electrodes resulting from ohmic drop in the solution (V = iR). This is a minor problem in highly conductive electrolytes, but in organic solvents specific resistivity is significant, reaching tens of megaohms even in the presence of 10^{-5} M electrolyte. For example, KCl at this concentration would have a specific resistivity of about 0.7 M? /cm. The amount of ohmic drop is relative to the amount of current passed between electrodes. Theoretically, open circuit potential measurements should be made at zero current, but unfortunately, no potentiostat is operating with such excellence. In reality, a small amount of current is being passed, and this introduces an error such that the actual potential is a bit higher (to the absolute value) than the one shown by the instrument. Additional error comes from the fact that the resistance path between the electrodes changes somewhat as the wire probe (working electrode) is moved. When the wire is well within the capillary, this problem may be negligible, but it likely takes on significance for positive "x" values, where the conductive path for the current between electrodes is progressively longer with increasing distance, hence, the underestimation is exacerbated.

Because the working and auxiliary electrodes are both made of the same metal (Pt), when the electrospray high voltage is switched off, the potential difference between the capillary and the wire is expected to be zero. However, at the end of an experiment with the solution still being pumped, a small potential difference is recorded even after the high voltage has been shut off. We consider this minor potential difference as the baseline to subtract out of the measurement, and attribute this phenomenon to differences

in the detailed structure of the two surfaces of the platinum conductors. The existence of such differences should probably not be surprising considering that different manufacturing methods were used in the respective fabrications. Minute differences in surface topography and accumulated contamination may cause different electrochemical responses from the two electrodes that are nominally made up of the same material.

Effect of Electrolyte Concentration. It is well known that a minimum conductivity in the introduced solution is necessary to initiate the electrospray process. Moreover, solutions with extremely low conductivities are known to produce very unstable Taylor cones[11]. On the other extreme, when solutions have excessively high salt concentrations, the problem of analyte signal suppression can be very severe in ES mass spectrometry[22,110,111] For this reason, we embarked on an investigation of the effect of electrolyte on measured open circuit potentials within the ES device. The potential gradient of 90/10 v/v acetonitrile/water solution, with $LiCF_3SO_3$ as a supporting electrolyte, was measured for three different electrolyte concentrations. $LiCF_3SO_3$ has been shown to exhibit only mild suppression of analyte signals in ES-MS[105,112]. The complete potential gradient profile for each solution is shown in Figure 3a.

It can readily be seen that as the supporting electrolyte concentration was raised, the potential difference was measurable to distances deeper within the ES capillary, with the highest ionic strength solutions yielding non-zero values at distances of over 15 mm away from the ES capillary exit. Coupled with this less rapid fall off is a lowering of the potential closer to the capillary tip for higher conductivity solutions. This is in agreement with the concept of controlled-current electrolysis where the ohmic resistance is the

determining factor in the distribution of the potential along the electrode. Thus, the higher numbers of charge carriers in solutions of progressively higher electrolyte concentration more effectively respond to the imposed high electric field, making the magnitude of the measured potentials higher at longer distances away from the counter electrode. Moreover, reducing the solution resistance enables the generation of faradaic current (resulting from oxidation processes at the ES capillary-solution interface) at deeper distances inside the capillary. Interestingly, the measured potential values very near the capillary exit show the exact opposite trend, i.e., the least conductive solutions give the highest values. The curve crossing near the ES capillary exit is thus a manifestation of the other side of the coin, namely that the least conductive solutions must attain the highest potentials to permit spray formation. It was also noted that at a fixed HV, increasing the salt concentration elongates the shape of the formed Taylor cone, leading to a cone-jet with a "curved generatrix"[33]. This implies that at the same positive "x" position, more solvent is present in front of the working electrode when the conductivity is higher. This alteration in the shape of the Taylor cone can contribute to a lowering of the measured potential at a given positive "x" value of the working electrode for solutions of higher salt concentration, because the distance from the working electrode probe to the tip of the cone strongly influences the measured value.

Additional experiments to verify the observed trends with varied salt concentrations were performed in redistilled acetonitrile; results appear in Figure 3b. Again the higher conductivity solution allowed measurement of non-zero potentials at significantly deeper penetration depths into the ES capillary, in this case, beyond 20 mm. The curves again cross near the ES capillary exit, indicating that the lower conductivity solution achieves

higher potentials in this zone. As occurred for 90:10 acetonitrile:water, elongation of the Taylor cone was observed for the solution of higher salt concentration in redistilled acetonitrile. Notably, at the constant voltage conditions used to generate both portions of Figure 3, the ES currents are expected to increase as the solution conductivity is raised[7,20,113]. This was verified by our own ES current measurements given in the Figure 3 caption. In considering all of these results, it can be concluded that the potentials measured near the ES capillary exit were highest for low conductivity solutions that were exhibiting the lowest ES spray currents. However, owing to elongation of the Taylor cone, higher conductivity solutions likely offer potentials closer to the highest levels observed for low conductivity solutions, as the Taylor cone tip is approached (see Figure 3b inset).

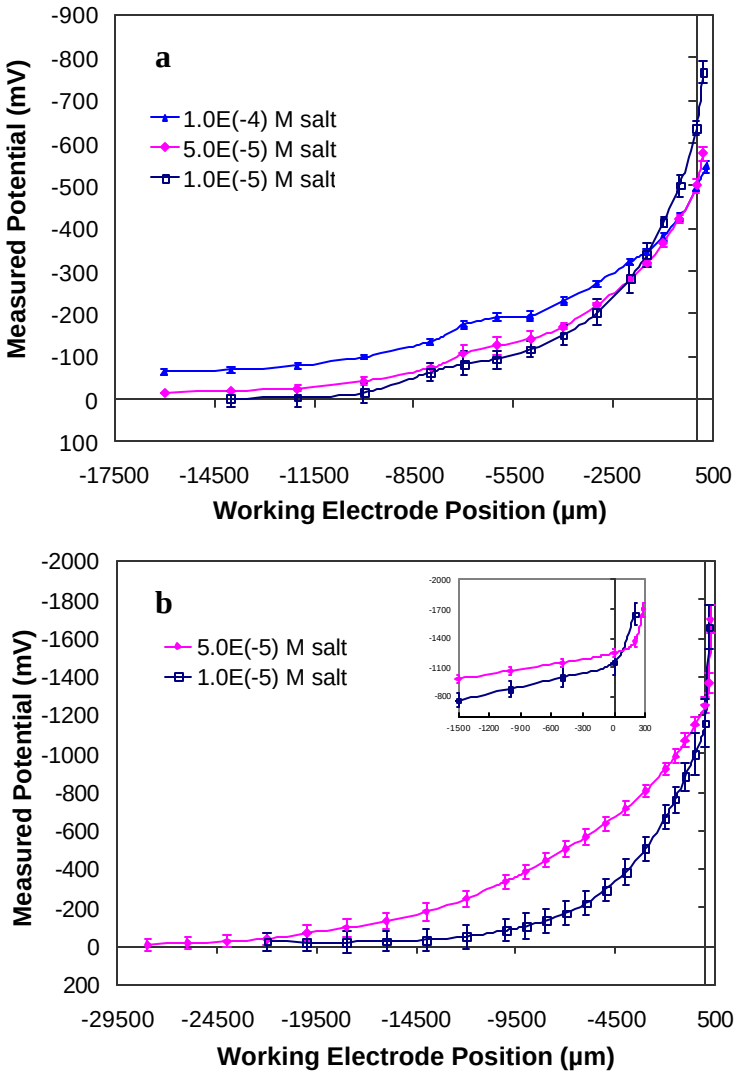

Fig. 3. One-dimensional DEEP maps generated from ES of: (a) 90:10 acetonitrile:water with varying salt concentration; HV = 3400 Volts; V_f = 250 µl/hr. The "0" point of the x-axis is indicated by a vertical line. In separate experiments, it was determined that at salt concentrations of 1.0 x 10^{-5} M, 5.0 x 10^{-5} M, and 1.0 x 10^{-4} M, the current from the ES capillary to ground was 55 ± 1 nA, 94 ± 1 nA, and 126 ± 2 nA, respectively; (b) 100% ACN with varying salt concentration, HV = 3600 Volts; V_f = 200 µl/hr. The solution with the higher salt concentration (1.0 x 10^{-5} M vs 5.0 x 10^{-5} M) maintained a higher ES current (39 ± 1 nA vs 89 ± 3 nA) as measured in separate experiments.

Effect of Solvent Oxidizability. To directly investigate the effect of solvent oxidizability on the shape of potential gradients near the ES capillary exit, two separate acetonitrile-based solutions were prepared. The first was pure, distilled acetonitrile, while the second utilized the same starting solvent that was diluted with 10% water; each contained 10^{-4} M electrolyte. Figure 4 shows maps of the potential profiles obtained using each solution. The potentials measured inside the Taylor cone are clearly higher at each point for the purified acetonitrile solvent than for the acetonitrile/water system. The curve originating from purified acetonitrile did not become totally flat even when the electrode was moved 14 mm into the emitter.

The oxidation of acetonitrile requires a significantly higher interfacial potential than the oxidation of water. In the absence of oxygen donors, acetonitrile oxidizes in a two-electron process to succinic dinitrile and hydrogen ions[114]. As the DEEP maps in Figure 4 demonstrate, at every working electrode position, much higher potentials are being established in dehydrated acetonitrile relative to the water-containing solution. Interestingly, in separate experiments where ES currents were measured for these same two solutions under conditions identical to those used to generate Figure 4, the spray currents gave only slightly differing values, i.e., 135 $\pm$ 2 nA for purified acetonitrile and 126 $\pm$ 1 nA for the 90:10 acetonitrile:water system. It is clear from Figure 4 that in the absence of water, potentials within the solution reach significantly higher values to achieve electrospray as compared to the situation where 10% water is present. We interpret this as a direct manifestation of the controlled-current nature of the ES device. The dearth of easily oxidizable material in the purified acetonitrile solution forces

potentials higher at all points along the capillary, and causes oxidation reactions to occur at the ES capillary/solution interface at points far deeper within the emitter.

Effect of Analyte Oxidizability. To further investigate the effects of solution components and notably the presence of readily oxidizable constituents, experiments were undertaken to compare DEEP maps obtained from purified acetonitrile solutions containing or devoid of an easily oxidizable compound, namely the polycyclic aromatic hydrocarbon rubrene. Rubrene readily undergoes oxidation ($E_{1/2}$ = 0.77 V vs. SCE in dichloromethane) to a resonance-stabilized radical cation. Figure 5 shows comparative results obtained from the two solutions which each contained 10^{-5} M electrolyte. The presence of rubrene clearly lowers the measured potential at all points along the capillary. The one-electron oxidation of rubrene occurs at substantially lower potential than the oxidation of acetonitrile, and must be presumed to be responsible for generating much of the charge excess in the sprayed solution. In keeping with the controlled-current description of the ES device, a purified acetonitrile solution forces the emitter to achieve much higher potentials in order to undergo oxidation to supply the ES current.

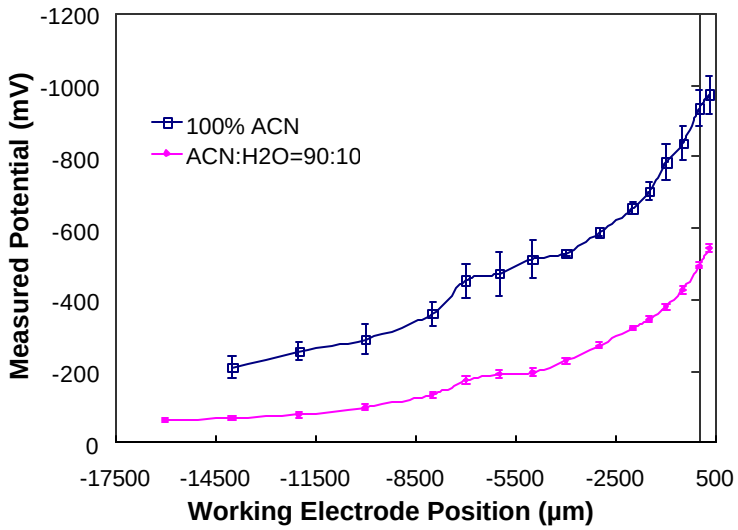

Fig. 4. One-dimensional DEEP map of 100% Acetonitrile vs. 90:10 Acetonitrile:water (each with 1.0 x 10^{-4} molar salt), HV = 3400 Volts; V_f = 250 µl/hr. The vertical line indicates the "0" point of the x-axis. The observation that 100% acetonitrile exhibited higher potentials than 90:10 acetonitrile:water at all working electrode positions near the ES capillary exit was quite reproducible.

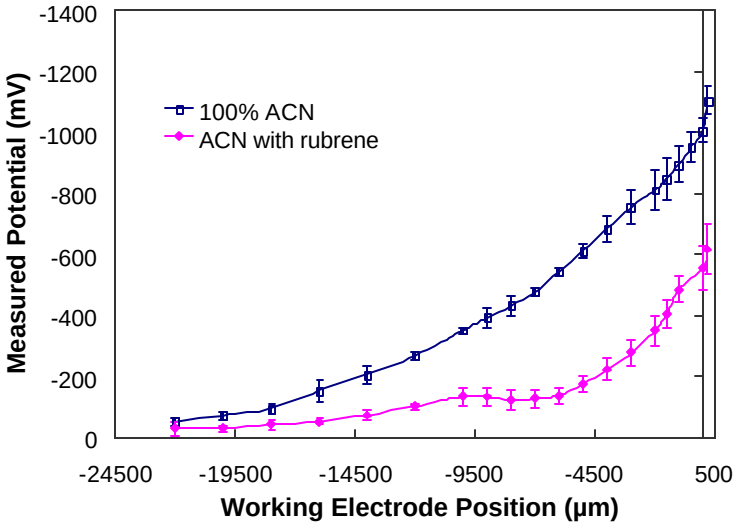

Fig. 5. One-dimensional DEEP maps of 100% acetonitrile with or without rubrene. HV = 3900 Volts; V_f = 200 µl/hr; salt concentration was 1.0 x 10^{-5} M; rubrene concentration was 2 x 10^{-5} M. The "0" point of the x-axis is indicated by a vertical line. ES currents for solution with and without rubrene were 71 ± 2 nA and 40 ± 2 nA, respectively.

Extrapolation of Relative Potential at Tip of Taylor Cone. The sharply increasing potential consistently observed with progressive movement into the Taylor cone for all solutions carries certain analytical implications. In the positive mode, the solution becomes progressively oxidative as the Taylor cone tip is approached. An analyte, impurity, product of electrochemical reaction, or any other molecule present in solution flowing toward the Taylor cone thus finds itself under increasingly oxidative conditions that allow the occurrence of solution-phase electron transfer reactions of progressively higher energies. All generated DEEP maps indicate that the potential reaches its extreme value only at the Taylor cone tip. While it is possible to move the internal wire probe electrode such that it enters the base of the Taylor cone (positive values on ordinate axis), at a certain positive value, the edges of the probe will actually touch the outer edges of the cone, causing the electrical contact between the electrodes through the electrolyte to be compromised. Under these conditions, it was visually observed that the spray actually starts to occur primarily from the protruding probe surface, and the potential of the working electrode attains very high values with respect to the ES capillary. Because of this limitation, reliable potential measurements were not possible at distances beyond about + 200-300 μm (depending upon the exact shape of the Taylor cone).

To allow estimation of relative potentials beyond this limit of physical placement, for the 1:1 methanol:water solution, we undertook the task of mathematical curve fitting with the goal of extrapolating potential values to the inaccessible region of the Taylor cone tip. Empirically, it was found that single exponential functions did not give satisfactory fits, but a biexponential growth function ($y = A_1*\exp[k_1 x] + A_2*\exp[k_2 x]$) was found to give a very reasonable result (Figure 6a). In a perfect, although grossly simplified situation,

due to ohmic resistance of the solution, the Faradaic current at the ES capillary drops proportionally with distance from the ES Taylor cone to the point of electron transfer at the ES capillary. Thus, the interfacial potential is the remainder of the applied potential (difference in potential between the anode and the cathode) minus the difference in the standard potentials of the anode versus the cathode, minus the ohmic drop between the electrodes. Because the overpotential at the electrode-solution interface is related to the Faradaic current through the Butler-Volmer equation, it would shape exponentially when plotted vs. distance from the cathode.

Closer inspection of the experimental data reveals that there are two almost distinct regimes of potential dependence, one external to the capillary and inside the Taylor cone, and another inside the capillary. This is explainable by noting that the geometry of the two areas is very different, hence, the current lines between the electrodes will have different shapes. Moreover, during ES operation, the entire metal end of the ES capillary is covered by solution. In such a situation, a large portion of the total oxidation may be occurring at the cut platinum end of the capillary (0.5 mm i.d., 0.6 mm o.d.). This surface is not only closest to the counter electrode, but also due to its roughness, it has an active area far exceeding the apparent geometrical area. The distinct differences between the field and current lines on the capillary's interior and exterior are likely to contribute to the bi-exponential nature of the behavior. Another probable cause is nonuniform conductivity of the solution. The concentration of charge carriers is somewhat higher in the Taylor cone, and smaller deeper inside the capillary, thus resistivity is not a linear function of distance between the electrodes.

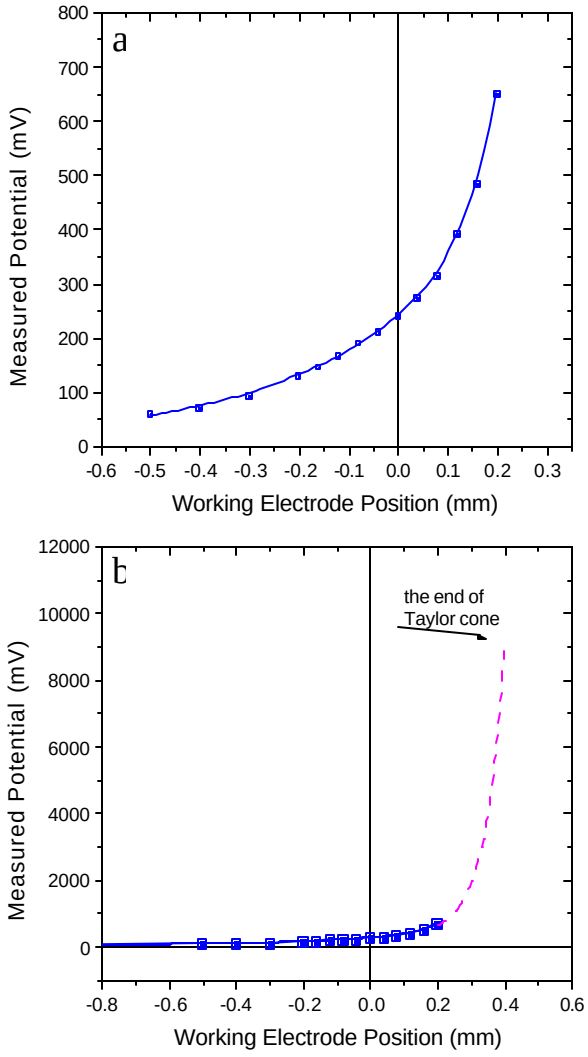

Fig. 6. (a) Curve fitting of 1:1 methanol:water DEEP map using bi-exponential function; (b) Extrapolation of open circuit potential to Taylor cone tip at +0.4 mm.

To use the above curve fitting to extrapolate the relative potential at the end of the Taylor cone, it is necessary to accurately determine the distance from the capillary exit to the Taylor cone tip. This was accomplished by using the accurately known outside diameter of the capillary to make a visual estimation of the distance to the tip of the cone. From such an estimate for the 1:1 methanol:water system, the cone tip was assessed to be 0.4 mm from the ES capillary exit. Extrapolation of the bi-exponential function to 0.4 mm to the Taylor cone tip gives an estimate of the order of 8 V (Figure 6b). Clearly, such an extrapolation makes certain simplifying assumptions, and small errors in the obtained data can result in large errors upon extrapolation. Visual inspection of the data from the numerical simulation done by Van Berkel[28] reveals a calculated interfacial potential of about 2.35 V at the ES capillary exit for water oxidation. It is obvious that the extrapolation shown in Figure 6b comes at some risk. When similar extrapolations were performed using DEEP maps generated from solutions of dehydrated acetonitrile or 90:10 acetonitrile:water, obtained values at the Taylor cone tip were of the order of single volts, in better agreement with the numerical simulations of Van Berkel.

Sources of Error in Measured Potential Values. For our two-electrode system, where the auxiliary electrode is simultaneously a grounded reference electrode, its potential is relatively stable within the course of the generation of an DEEP potential map. The potentials measured at the working electrode are relative to this ground and are reported without correction for ohmic drop, which, in low conductivity solutions, has a non-negligible value. For measurements made at positive x-axis values, the resistance between the electrodes is higher than for those made at negative x-axis values, and the

resistance clearly increases as the probe penetrates further into the Taylor cone. Error also comes from uncertainty in the standard potentials of reactions taking place on either platinum surface. This matter is largely under-appreciated outside the electrochemical community, but it is well known that the history (e.g., irreversible oxidation after imposition of high potentials) and topography (e.g., reconstruction and polycrystalline structure) of platinum surfaces play very important roles in the actual mechanisms of the reactions and their standard potentials. For these reasons, the applicability of a general form of the current-potential relationship, especially for non-Nernstian irreversible organic systems in which adsorption or dissociative adsorption must precede electron transfer, is not evident.

We also recognize that perturbations on measured potentials are caused by the introduction of the working electrode probe itself (wire and shielding) that occupies a large portion of the capillary orifice. Its presence alters flow conditions relative to an unobstructed capillary, but it is difficult to assess the error caused by an imperfect (non-laminar) hydrodynamic flow. It is possible that some stagnant (or less dynamic) areas are formed around the probe shield, thereby slowing access of sample constituents to the working electrode. The magnitude of this error will vary depending on the position of the working electrode. This problem can also contribute to a slow drift to stable potentials.

When the working electrode probe is moved, the active area on the ES capillary surface changes, as does the current density distribution near the surface, which in turn, changes the distribution of the interface potential. Probe movement also affects the available volume that electrochemically-active reactants and products will occupy. Because electricity is conducted through a certain volume of electrolyte, resistance of the

electrolyte between the two electrodes is higher to positions behind the working electrode relative to those in front of it. Because of this imbalance and the resulting restricted transport from areas behind the electrode, less current can flow from the deeper regions, and this must be compensated for by a higher current from points in front of the working electrode. This will cause interfacial potentials at points in front of the working electrode to reach higher values than they would reach in the absence of the probe. In a sense, the probe compresses the available surface for electrochemical reaction by favoring the area in front of it.

Conclusions

Differential Electrospray Emitter Potential (DEEP) mapping of potential gradients near the electrospray exit invariably showed a monotonic descent from the highest measured potentials nearest the Taylor cone tip, to a flat gradient within the capillary. The absence of easily oxidized species in the spraying solution caused measured potentials to reach higher values near the Taylor cone, while also extending the measurement of non-zero values to positions deeper inside the capillary. Removal of species with low oxidation potentials thus effectively raised the entire measured potential curve at all distances. This result is in keeping with the description of the ES device as a controlled-current electrolytic cell. An increased concentration of electrolyte also extended the distance within the capillary that a non-zero potential difference was measurable. A higher conductivity solution thus effectively extended the influence of the applied high voltage to deeper distances within the capillary, and electrochemical oxidation was presumably occurring at deeper distances. Conversely, the solutions with lower conductivities

exhibited higher measured potentials near the capillary exit, indicating that most of the current was generated very near the exit.

These results will find application for an analyst who seeks to ionize a compound that lacks nucleophilic sites and is therefore unresponsive to proton or other cation attachment. In this situation, one may increase the ES-generated yield of radical cations of such a compound by removing solution species that are more readily oxidized. Furthermore, the existence of very high potentials in the solution near the capillary exit indicates that chemical (redox) reactions are likely to take place in solution, in and near the Taylor cone. Our data suggest that the electrochemical "stress" (oxidative in positive ion mode experiments) may be substantially higher than any previous studies indicate. This implies that reactions that were previously thought of as taking place via Faradaic electron transfer at the metal solution interface may, in fact, be occurring in solution as EC type reactions.

Acknowledgments

Financial support for this research was provided by the National Science Foundation through grant number CHE-9981948. The authors thank Bruker Daltonics, Inc. for supplying electrospray source parts.

CHAPTER 2

Shifts in Peptide and Protein Charge State Distributions with Varying Spray Tip Orifice Diameter in Nano-electrospray FT-ICR Mass Spectrometry

Yan Li and Richard B. Cole*

Department of Chemistry, University of New Orleans,
2000 Lakeshore Dr., New Orleans, LA 70148

Abstract

The influence of the diameter of the spray tip employed for nano-electrospray mass spectrometry (nano-ES-MS) upon mass spectral charge state distributions was investigated using angiotensin I (m_r = 1296), insulin (m_r = 5774), and ubiquitin (m_r = 8560) as test analytes. Under a variety of experimental conditions, the charge state distributions of the test peptides and protein consistently shifted toward higher values as the tip orifice diameter decreased. This finding indicates that the use of narrow diameter capillaries can promote the formation of higher charge state ions that are more reactive precursors in tandem mass spectrometry experiments. A detailed comparison of charge state distributions obtained for nanospray capillaries of varying diameters was undertaken while systematically varying experimental parameters such as sample flow rate, analyte concentration, solvent composition, and electrospray current. The general tendency to obtain higher charge states from narrow diameter capillaries was conserved throughout, but tips with smaller orifices were more sensitive to sample flow rate (the average charge state was lowered significantly as flow was raised), while tips with bigger orifices were more sensitive to analyte concentration and pH of the solution (as each was lowered, the average charge state increased).

*Author to whom correspondence should be addressed

Introduction

One distinguishing characteristic of electrospray mass spectrometry (ES-MS) is the propensity to form and detect multiply charged analyte species which enables observation of macromolecules at relatively low m/z values[29-31]. Not only does the ES process make the detection of large biomolecules possible, but in addition, the charge state distribution of the analyte can serve as a probe to monitor its conformational dynamics[32-36]. Several models have been built to depict the details of the ionization process in ES-MS[36-41], and a better understanding of the factors that influence the analyte charge state distribution can help to clarify mechanistic aspects of the ES process. It has been shown that the analyte structure/conformation[33-35,42,43], analyte concentration[36,40,44-46], gas-phase reactivity[47-55], solution pH[32,53,56-60], solvent composition[61-63], and ES instrumental parameters[48,50,64,65], all have influences on the final charge state distribution observed in ES-MS.

More recently developed nano-electrospray (nano-ES) is different from conventional electrospray (the latter typically employs 4-200 microliter/min flow rates through 0.1 mm diameter capillaries) in that the employed nanospray tips have very small orifices, usually less than 10 μm in diameter[38], and flow rates are in the 10-500 nL/min range. Compared to conventional ES, there are several advantages that make nano-ES very attractive: 1) the onset of ES occurs at a lower applied voltage which helps to reduce the problem of electrical (corona) discharge; 2) because the sample flow rate is so low, much less sample is consumed; 3) the radii of initially produced droplets are smaller so the ionization efficiency is higher; 4) nebulizing gas and drying gas are not necessary, so ion transmission is higher[66]. Furthermore, it is believed that the low solvent flow rate affects the mechanism of ion formation. Mann et al.[67] theoretically described the electrostatic

dispersion in nano-ES. Karas et al.[68] presented a model to explain the origin of the different mass spectral characteristics of ionspray and nanospray by suggesting different "predominant fission pathways" depending on the size of the initial droplets. They point out that ions with low surface activities experience greater losses to the residue during fission events while the more surface active species become enriched. In nanospray, because ions are desorbed from smaller initial droplets that presumably undergo fewer fission events, Karas and coworkers[69] reasoned that analytes with lower surface activities (e.g., oligosaccharides, glycosides and glycoproteins) would experience higher transmission through the ion source, as compared to conventional electrospray.

Nanospray emitters also exhibit certain drawbacks such as fragility, causing a high propensity to fracture the sharp end of the tip. This is because, unlike the emitter used in conventional ES that is typically made of stainless steel, nanotips are usually made of glass that is coated with a conductive metal. Also contributing to the short lifetimes of nanotips are the problems of corrosion of the conductive coating, and sample clogging[70]. Another issue is that, owing to manufacturing difficulties, the orifice of the nanotip is less uniform than in conventional ES.

The ability to obtain reproducible charge state distributions can have an enormous impact on the accuracy of studies that rely on a single charge state for quantification. In addition, MS/MS studies performed on multiply charged precursors require a minimum signal for the selected precursor ion. The success of such tandem mass spectrometry experiments can hinge on the ability of the analyst to control conditions to favor the production of ions of specified charge states. For a given precursor molecule, ions of higher charge state are known to undergo decompositions more readily than those of lower charge state[48,49,71,72].

Moreover, because attempts have been made to use nano-ES-MS to probe the binding and conformational properties of noncovalent complexes[73], the exact nature of interactions may change as the charge state shifts. For these reasons, it is important to obtain a detailed understanding of the effects of the physical characteristics of the nanospray tip on the charge state distributions of analytes.

Experimental Section

All experiments were performed in the positive mode on a Bruker (Billerica, MA) 7.0 T Fourier transform ion cyclotron resonance mass spectrometer (FT-ICR-MS). The electrospray source was an Analytica of Branford (Branford, CT) model 104444 with API 100 controller equipped with a nanospray accessory (Bruker #MS0102) that uses neither nebulization gas, nor counter-current bath gas. The spray tips are aligned off-axis with respect to the metal-coated entrance capillary that serves as the counter electrode. Nanospray tips were purchased from New Objective (Woburn, MA). Angiotensin I, insulin, and ubiquitin were purchased from Sigma (St. Louis, Mo) and were used without further purification. Solutions were prepared by dissolving samples in methanol/water in a 1/1 ratio on a volume/volume basis. For all presented plots, each point represents the average of three measurements, and error bars show the standard deviations of the three measurements.

The capillary exit voltage (**capexit**), the DC offset of the hexapole ion guide (**offset**), and the ejection time of ions from hexapole to analyzer (**P2**) all have noticeable effects on the charge state distribution. Generally, higher values of these parameters favor lower charge states (data are not shown). These parameters mainly affect ion transmission through the hexapole ion guide. In our experiments, these parameters were held constant at values

which give relatively stable and strong signals, **capexit** = 80 V, **offset** = 2.57 V, **P2** = 3000 μSec.

Results and Discussion

The mechanism of ion formation, and discrimination effects in ion transfer and possibly even ion detection, can affect the charge state distribution observed in an ES mass spectrum obtained for a given analyte. To test the effect of physical characteristics of the tip orifice on the charge state distribution, it is important that every instrumental parameter remains constant as the tip orifice properties are varied. In our FT-ICR system, parameters for ion transfer and ion detection can be precisely set via computer-controlled electronics. The only parameter that needs to be adjusted manually is the distance (**d**) between the nanospray tip and the counter electrode. The value of **d** read from the micrometer of the nanospray device for all experiments was 0.3 cm. Although this value cannot be read to a high number of significant figures, with a fixed micrometer setting, it is nonetheless highly precise (reproducible) and constant for all experiments.

In loading the same solution into different tips having orifices of variable size, it is impossible to keep both the applied high voltage on the counter electrode (**HV**) and the electrospray current (**ESC**) constant simultaneously. Because **ESC** is a measurement of how much excess charge is present in the ES process[40,41,115], we chose to maintain a fixed distance between the nanospray tip exit and the counter electrode, and then set the **ESC** at a fixed value (either 50, 20 or 10 nA, as indicated) by adjusting the **HV** upon introducing a new nanospray tip.

The weighted average charge state (**ACS**) has been used to evaluate the charge state distribution[35]. It is given by equation 1.

$$\mathbf{ACS} = \Sigma \mathbf{N_i I_i} / \Sigma \mathbf{I_i} \qquad (1)$$

Where $\mathbf{N_i}$ is the number of charges on each peak representing the intact molecule, and $\mathbf{I_i}$ is the absolute intensity of each peak.

Evaluation of nanospray tip diameter. To investigate the effect of changing the tip orifice diameter on the charge state distribution, three types of nanospray tips were purchased (New Objective) with nominal inner diameters (ID) of 1 μm, 2 μm, or 4 μm. A JEOL (Peabody, MA) JSM-5410 scanning electron microscope was used to measure the exact width of the orifice at the spray tip after mass spectrometric data had been acquired. Obtained SEM images of three employed nanotips are shown in Figure 1. The measured ID range for three types of nanotips were 0.9 ± 0.2 μm, 2.2 ± 0.3 μm, 5.2 ± 0.8 μm, referred to as #1 μm tip, #2 μm tip, and #5 μm tip, respectively (Fig. 1).

Electrospray current (ESC) value as a consequence of applied high voltage (HV). To optimize the electrospray current, both the signal intensity and the signal stability must be considered. To examine the effect of a changing electrospray voltage on the electrospray current at fixed distance between tip and counter electrode, a 20 μM angiotensin I solution was loaded into the nanospray tip. Figure 2 shows the ES current variation as a function of the high voltage applied to the counter electrode; a mass spectrum was acquired at each point. Currents are quite stable when they are between 10 nA and 70 nA.

50 nA was chosen as the **ESC** value used in subsequent experiments unless specifically indicated otherwise.

It is interesting to note that in Figure 2, ES currents for the #1 μm tip are larger than those of the #2 μm tip at every applied high voltage, although perhaps electric (corona) discharge occurred for the #1 μm tip when the **HV** was higher than 900 V. The 1 μm tip has a different coating material and style as compared to the #2 μm and #5 μm tips[51] which can contribute to a change in the current-voltage relationship (the #1 μm tip has a single-layer coating, while the #2 μm and #5 μm tips have multilayer coatings, which render them more durable). Another possible reason for this apparent anomaly can be found from Pfeifer's equation[116]:

$$I = [(4\pi/\varepsilon)^3 (9\gamma)^2 \varepsilon_o{}^5]^{1/7} (KE)^{3/7} (V_f)^{4/7} \qquad (2)$$

Here I = ES current; ε = permittivity of solvent; γ = surface tension of solvent; ε_o = permittivity of vacuum; K = conductivity of solution; E = applied electric field at capillary tip; V_f = flow rate. For all employed spray tips, ε, ε_o, γ, and K are constant, while V_f increases with the diameter of the tip orifice. According to Pfeifer's approximation[116], E is smaller for a tip having a bigger orifice.

$$E = 2V_c / [r_c \ln(4d/r_c)] \qquad (3)$$

Where V_c = applied potential; r_c = capillary outer diameter; d = distance between spray tip and the counter electrode. The combined effects (lower E but higher V_f for larger orifices) are somewhat offsetting, and can result in a slightly lower ES current for the #2 μm tip than for the #1 μm tip (see calculation in appendix A).

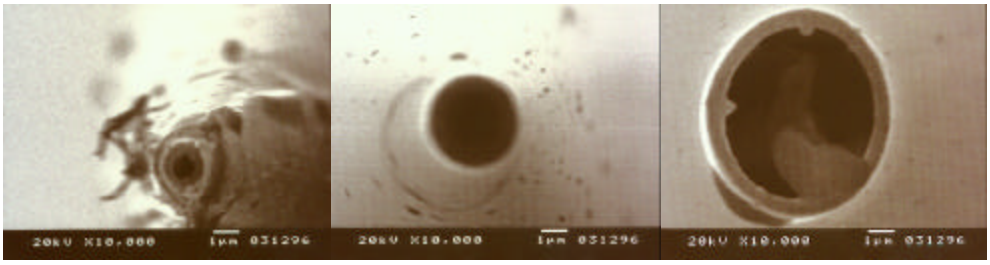

Fig. 1 Scanning electron microscopy images of employed nanospray emitters: (a) #1 um tip; (b) #2 um tip; (c) #5 um tip. Images were obtained after approximately two hours of use.

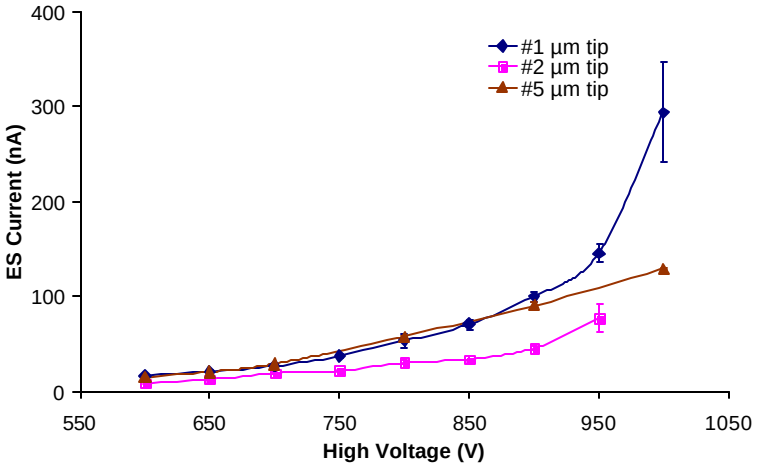

Fig. 2. Electrospray current (**ESC**) vs. applied high voltage (**HV).** The employed solution was 20 µM angiotensin I in methanol/water (1/1) solution. Error bars indicate the standard deviations of three repeated measurements.

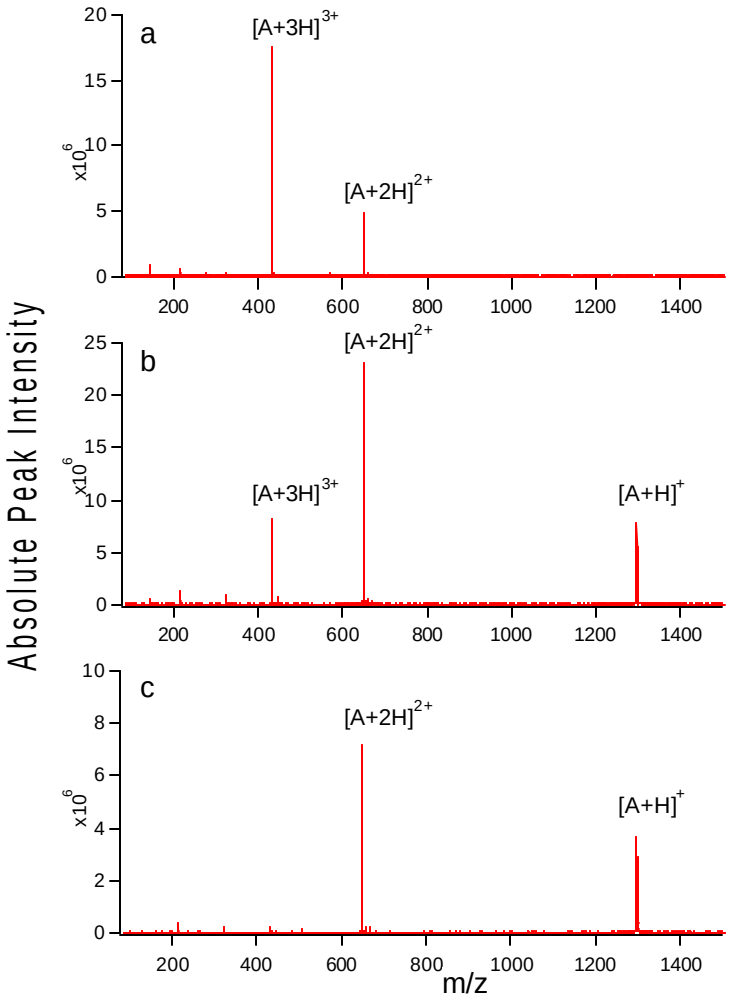

Fig 3. Nano-ES mass spectra of 20 µM angiontensin I loaded into: (a) #1 µm tip; (b) #2 µm tip; (c) #5 µm tip. The solution and employed experimental parameters (including distance between tip exit and counter electrode) were held constant. Only the applied high voltage was adjusted to obtain a fixed current value of 50 nA at the emitter tip.

Effect of tip orifice diameter on weighted average charge state (ACS). Figure 3 shows mass spectra of 20 μM angiotensin obtained using three different spray tip orifice diameters. When using the #1 μm tip, the peak representing triply charged ions was dominant. For the #2 μm tip, doubly charged ions gave the strongest peak. When the #5 μm tip was employed, the peak corresponding to singly charged ions became very strong, while the peak representing triply charged ions almost disappeared. The weighted average charge states calculated from the data in Figure 3 are plotted in Figure 4a. The trend is very apparent that as the tip orifice diameter increases, the **ACS** of 20 μM angiotensin I decreases. These data illustrate the dramatic influence that the diameter of the employed nanospray tip can have on the distribution of observed charge states.

In analyses where tandem mass spectrometry is required, it may be highly advantageous to improve the yields of highly charged ions at the expense of those of lower charge states. In this manner, precursor ions of higher reactivity can be obtained[48,49,71,72], hence, the yields of product ions can be improved, and the variety of decompositions that are accessible can be widened, especially at the higher energy end. Our results indicate that the use of nanotips of narrower diameter can lead to this type of spectral enhancement. Conversely, if one seeks to simplify product ion spectra by augmenting the intensity of, and then mass-selecting, singly charged precursor ions such that only singly charged products are obtained, the use of wider diameter capillaries would be more appropriate.

In further experiments using more dilute angiotensin I (2 μM), the trend remained the same, although the drop off was much attenuated (Fig. 4a). To expand the number of tested examples, a 2 μM ubiquitin (m_r = 8560 Da protein) solution was also studied. Due to severe clogging, #1 μm tips could not be used; instead, the #2 μm, #5 μm, and

intentionally broken #5 μm tips (giving orifice diameters much larger than 5 μm) were employed. The ubiquitin results (Fig. 4b) echo those of the shorter peptides with the larger tip diameters yielding lower **ACS** values.

Effects of flow rate. To shed further light on the underlying reasons why the **ACS** of the analyte changes as a function of nanospray tip ID, we looked closely at the flow rate as the tip orifice diameter was changed. We noticed that even when the ES current was held constant, the sample flow rate during ES changed substantially when the tip ID was altered. However, there is no convenient device to measure the exact value of the flow rate. Instead, we used positive pressure of N_2 gas to push the solution out of the tip at a faster rate than it naturally flows. By controlling the gas pressure, a coarse control of the flow rate was obtained. As the gas pressure was raised, the MS signal intensity decreased and the charge state distribution of the analyte became less reproducible. This problem was more serious for the #5 μm tip. When the gas pressure became larger than 6 psi, usually no MS signal remained. To enable stable signals over the entire range of flow rates while the flow was forced faster, the **ESC** for this series of experiments was fixed at 10 nA. The **ACS** of 20 μM #1 angiotensin was observed to decrease as the gas pressure (psi) increased (Fig. 5a).

To measure the approximate flow rate, we first calibrated the nanospray tip by loading solution in increments of 1 μL while marking the load level at each increment. We then started the ES process and recorded how long it took for 1 μL of solution to be consumed. Subsequently N_2 gas was applied at a certain pressure, and the time it took for the next 1 μL solution to pass was recorded. The measurement was repeated at a different gas

pressures. To avoid the problem of tip clogging, we used neat methanol/ water 1/1 as the sample solution (no peptide or protein). Table 1 gives the flow rate as a function of pressure, measured in this manner. The **ESC** for this series of experiments was fixed at 20 nA. Figure 5b shows how the **ACS** of 20 μM neat angiotensin solution changed as a function of flow rate. A clear decrease in **ACS** values with increasing flow rate was detected in all flow regimes. From this figure, it is evident that sample flow rate is a main factor that influences the obtained charge state distribution of angiotensin.

This result is consistent with a consideration of the ratio of excess charges to analyte molecules as expressed in the N/N_0 quotient introduced by Wang et al.[12]. When N is the total number of excess charges, and N_0 is the total number of analyte molecules, the N/N_0 quotient is given by:

$$N/N_0 = (I / e) / (ACV_f) \qquad (4)$$

where I is the ES current (C/sec); e is the elemental charge; A is Avogadro's constant; C is analyte concentration (mol/L); and V_f is the solution flow rate (L/sec). Because I and C are set at constant values while e and A are fixed constants, N/N_0 will decrease as V_f increases. As the tip orifice increases from 1.0 μm to 2.2 μm to 5.1 μm, the flow rate increases from about 1.3 nL/sec to about 2.0 nL/sec to about 5.3 nL/sec. Over this interval, N/N_0 will decrease by a factor of 4 (see calculation, Appendix B). In other words, there are the same number of excess charges for an increasing number of analyte molecules, so the **ACS** of angiotensin decreases.

Effect of analyte concentration. It has been shown that for multiply charged analytes, increasing the analyte concentration generally will shift the charge state distribution

toward lower values[12,16,17]. It is believed that with higher concentrations, an increase in the competition among analyte molecules for the available excess charges on the droplets results in fewer ions bearing higher numbers of charges. Using a #5 μm tip and the previously described fixed operating conditions, the **ACS** of 2 μM angiotensin was calculated to be 2.60, while the **ACS** of 20 μM angiotensin was 1.65 (Fig. 4a). The drop off is thus about 1.0 unit. Using a #2 μm tip, the **ACS** of 2 μM angiotensin was 2.81, while the **ACS** of 20 μM angiotensin was 1.98; hence, this drop-off was about 0.8 units. However, for #1 μm tips, changing the concentration from 2 μM to 20 μM only decreased the **ACS** from about 2.87 to 2.79, i.e., less than 0.1 units. The work by Chowdhury et al.[16], Smith et al.[17], and Wang et al.[12] focused on conventional ES (higher flow regime) and not on nanospray. Their conclusions regarding the effect of increasing the analyte concentration on the obtained charge state distribution are still likely to be applicable, but they appear to be attenuated to a large degree. It seems that when the tip orifice becomes very small, in the tested concentration range, analyte charging is so facile that even a ten-fold increase in the concentration of this analyte only slightly decreases the obtained **ACS**. In other words, in the lower flow regime obtained with the #1 μm tips, the ratio of excess charges (N) to analyte molecules (N_o) may be high enough such that an increase in analyte concentration only slightly alters the ability for the analyte to attract, on average, three protons.

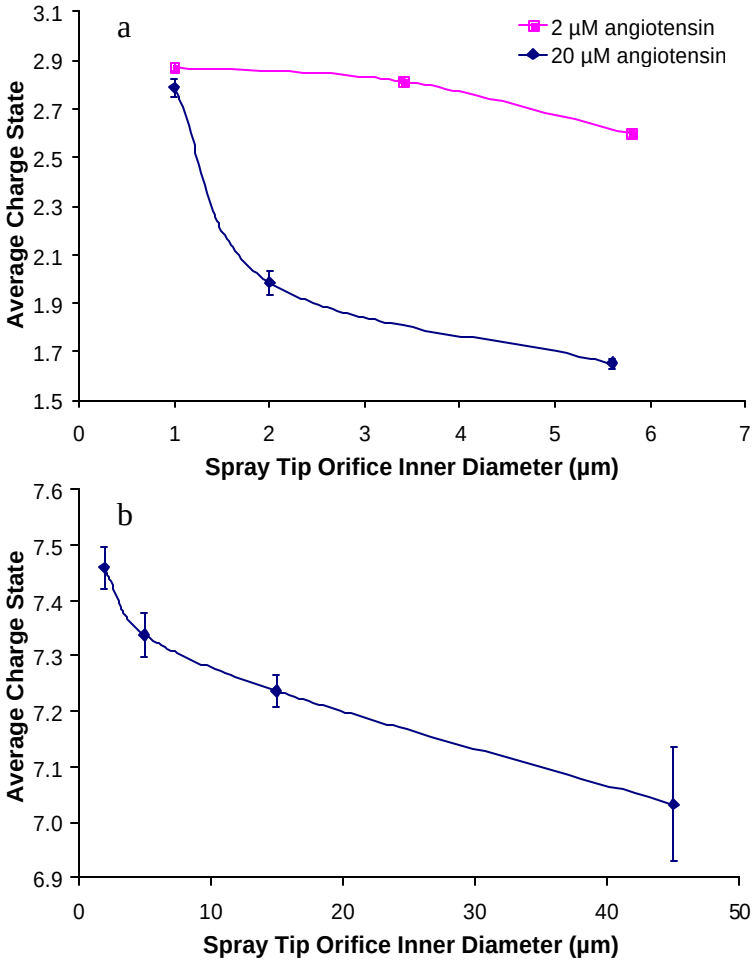

Fig. 4. The weighted average charge state (**ACS**, see text) vs nanospray tip orifice inner diameter of : (a) 20 µM and 2 µM angiotensin in neat MeOH/H_2O (1/1) solution; (b) 2 µM ubiquitin in MeOH/H_2O (1/1) solution. Exact tip orifice diameters were determined by scanning electron microscopy. In pane (b) only, the two largest tip diameters were achieved by intentionally breaking #5 µm spray tips. The resulting surfaces suffered from some irregularity and the inner diameters were estimated to be 15 ± 3 µm and 45 ± 5 µm.

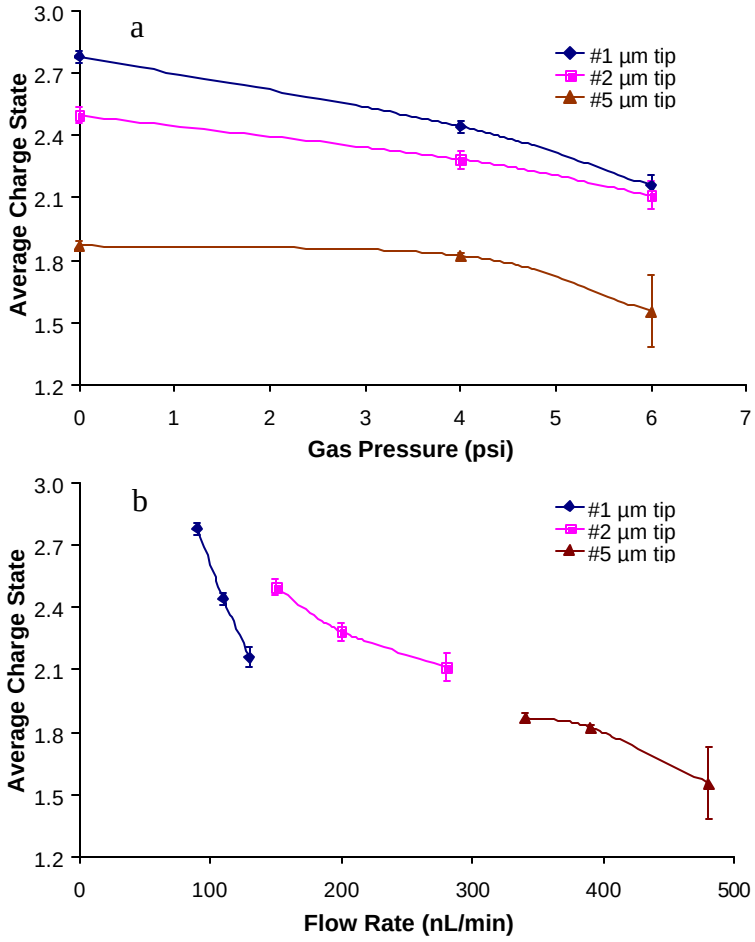

Fig. 5. Weighted average charge state of 20 µM angiotensin I as a function of : a) gas pressure; b**)** flow rate. Error bars indicate the standard deviations obtained from three measurements.

Effects of employed buffer. When studying proteins or peptides using ES-MS, solvent additives such as 1% acetic acid or mM levels of ammonium acetate are often used. To test the influence of selected solvent additives on the magnitude of the shift in the **ACS** observed as a function of a changing nanospray capillary diameter, three solutions were prepared (neat, buffered, and acidified). Figure 6a shows the changes to the **ACS** values of the three angiotensin I solutions described in the figure legend, as a function of variable tip orifice diameter (#1 μm, #2 μm, or # 5 μm tips). Although still present, compared to the trend of the neat solution, the **ACS** drop-offs for buffered and acidified solutions are less dramatic.

It has been noted and discussed that increasing the acidity of solutions can produce a higher degree of solution protonation of proteins in a given conformation, and cause unfolding of proteins at low pH. Both of these phenomena can contribute to an increase of the **ACS**. In the current experiment, the contribution of conformational change at low pH is negligible. First, angiotensin I is a rather small peptide. Second, all solutions were initially prepared in 50% methanol, whereby any denaturing effect of methanol on the conformation of angiotensin I will be constant. Adding in 1% acetic acid to a 1/1 methanol/H_2O solution will increase the proton concentration to about 5.9 x 10^{-4} M[117]. Using the #5 μm tip, the **ACS** of this acidified solution was found to be about 1.0 unit higher than that of the neat solution. When the tip ID was approximately 1.0 μm (#1 μm tip), the **ACS** values of acidified and neat solutions were almost the same. This finding reinforces our rationalization that as the tip orifice is decreased to about 1.0 μm (the lowest flow rate situation), the number of protons available as excess charges is already so high compared to the number of analyte molecules that the extra number of protons

(with counter ions) made available by lowering the pH does not affect the **ACS** to a large extent.

It has been reported that an increase in the concentration of ammonium acetate caused a slight decrease of the **ACS** of lysozyme[35]. The pH increase was likely to contribute to the decrease in **ACS** upon addition of ammonium acetate to lysozyme solution. In the present experiments, the **ACS** obtained in buffered solution is generally about 0.9 units lower than that found using the acidified solution. The basicity of ammonium acetate likely favored the removal of protons from angiotensin. Moreover, when an ammonium ion (NH_4^+) is the charge carrier attached at a basic site on angiotensin in place of a simple proton (H^+), loss of NH_4^+ from this adduct (heavily favored over loss of a bare proton) will cause the **ACS** to drop off more precipitously as compared to the case where no ammonium acetate is present[53].

To further test the effects of the employed buffer on an obtained analyte charge state distribution, three solutions of insulin were prepared, each at 2 μM. Insulin was either neat, buffered, or acidified, and the three solutions were run under identical instrumental conditions; results are shown in Figure 6b. Although trends are less pronounced, they maintain the same directions as those for angiotensin I (Fig. 6a). The **ACS** of the acidified solution is slightly higher than that of the neat solution, and about 1.0 unit higher than that of the buffered solution. The **ACS** difference between the acidified and the neat solution is less pronounced when the tip orifice has a smaller diameter.

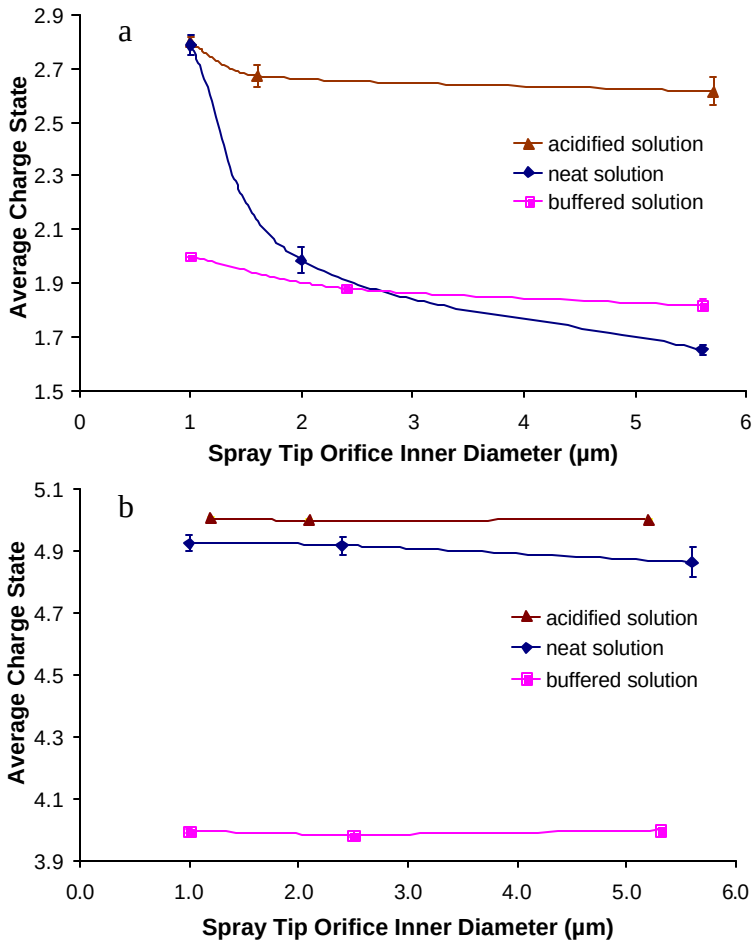

Fig. 6. Weighted average charge states observed in test solutions of three different compositions vs. increasing nanospray tip orifice diameter: (a) 20 µM angiotensin I (b) 2 µM insulin. For each analyte, "neat solution" consisted of methanol/water (1/1); "buffered solution" contained 5 mM ammonium acetate in methanol/water (1/1); and "acidified solution" contained 1% (vol) acetic acid in methanol/water (1/1).

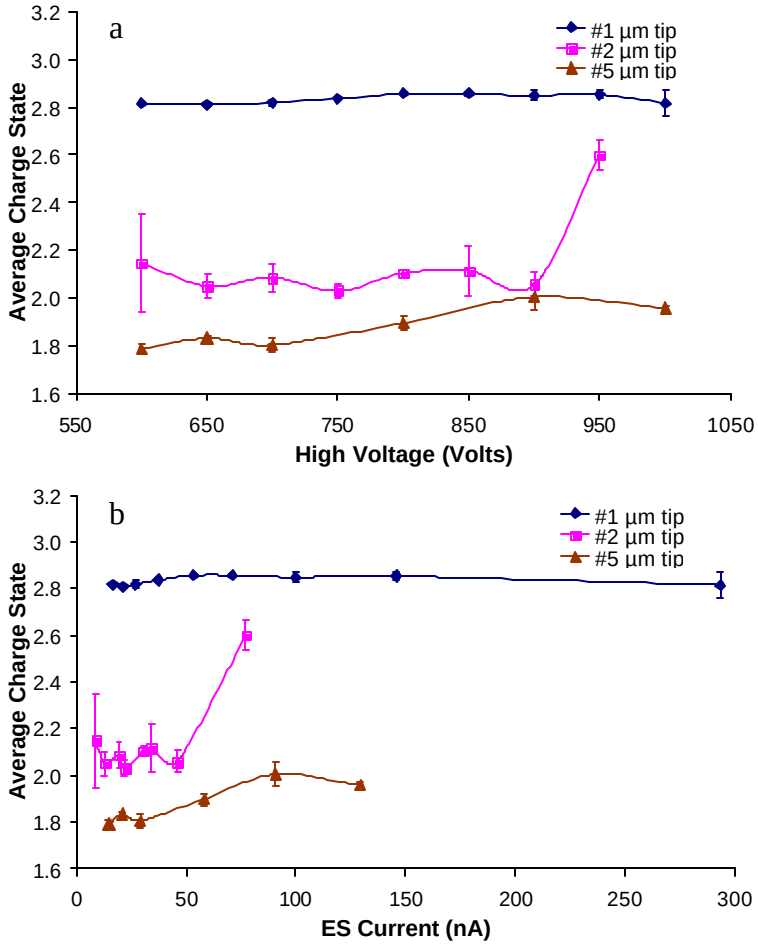

Fig. 7. The weighted average charge state of 20 µM angiotensin I as a function of : (a) applied high voltage; and (b) ES current.

Effects of variable ES current

Because the distance between the counter electrode and the nanospray tip is held constant, an increase in the high voltage will result in an increase in the ES current. Fig. 2 showed the **ESC-HV** response curve of 20 μM angiotensin loaded in tips of different IDs. As the **HV** was raised from 600 V to 1000 V, in response, the **ESC** increased from 10 nA to more than 100 nA (example of #5 μm tip). Over this interval, N/N_0 increases by about a factor of 10. Van Berkel and coworkers[118] have shown that H^+ is a principal oxidation product formed at the metal-solution interface when methanol/water solutions are employed as the ES solvent. If the primary product of the inherent electrochemistry in ES-MS was production of protons, then one would expect the **ACS** of angiotensin to undergo an obvious increase as the high voltage (and ES current) increased.

The experimental results shown in Figure 7 do not seem to support this expectation. The plots shown in Fig. 7a and Fig. 7b are generated from the same three sets of data. Figure 7a plots the **ACS** vs the applied high voltage, while Fig. 7b shows the **ACS** vs the ES current. The **ACS** of angiotensin stays virtually constant over the entire current range when employing the #1 μm tip, and there are only slight increases when using the #2 μm tip or the #5 μm tip, in response to the dramatic increase in ES current. Even at very low ES current (10 nA), N/N_0 for an initial droplet formed from the #1 μm tip is about 4.0 (see appendix B). During all of the conducted experiments, however, the $[A+4H]^{4+}$ peak never increased noticeably, even when 1% acetic acid was added. There are three basic amino acid residues in the sequence of angiotensin I (DRVYIHPFHL) plus the N-terminus whose ability to capture a charge will be impeded by a nearby protonated arginine. If for angiotensin I, a significant coulombic barrier exists between the +3 and

+4 states such that the methanol solvent is in competition for the fourth proton[121], more excess charges in the solution or in the droplet will not raise the **ACS** to a great extent, regardless of how many more excess charges are produced by the ES current increase. According to the model of Mann and Wilm[38], a typical diameter of a droplet emanating from a nanospray emitter is less than 200 nm at a flow rate of 20-40 nL/min. At analyte concentrations of 1 pmol/μL (= 1 μM), such droplets contain one analyte molecule on average. So, in our experiments using 2 μM angiotensin for the #1 μm tip, on average, there are about two molecules in each droplet. No matter how many excess charges are present in the droplet, the charges the molecule can accommodate is limited by the number of basic sites on the molecule and their basicity relative to the employed solvent, and by coulombic repulsion. So an increase in ES current does not greatly affect the observed **ACS**.

Unfortunately, this reasoning cannot explain the data acquired with the #2 μm tip and the #5 μm tip, where the **ACS** values are considerably lower than +3. The **ACS** of angiotensin did not increase at all for the #2 μm tip as the **ESC** increased from 8.8 nA to 46 nA. For the #5 μm tip, it increased by less than 0.2 units as the **ESC** went from 14 nA to 130 nA. Because charging of angiotensin arises from excess protons, these latter findings are likely an indicator that the number of available protons does not increase proportionally with the increasing current. However, the ES current has been defined as the mathematical product of [(average number of charges per droplet) x (the rate of formation of charged droplets)][40]. Theoretical equations[116,119] and experimental data[39] all indicate that the ES current value is proportional to the sample flow rate. This means that the rate of formation of charged droplets will increase as the ES current value is raised.

Pfeifer and Hendricks' model[116] predicts that the radius of the droplet (R) is proportional to $(V_f)^{2/7}$, while de la Mora and Locertales[119] give R as proportional to $(V_f)^{1/3}$. A third model, that of Mann and Wilm[67] dealing specifically with nanospray emitters, predicts a proportionality between the flow rate and the size of the droplets emitted from the nanotip as $(V_f)^{2/3}$. Despite differences in the value of the exponent, all three models indicate that R increases with V_f. Thus, as the ES current increases, not only does the charge available to droplets increase, but the average droplet size also increases, as does the solution flow rate. The overall result is the formation of larger droplets that hold a higher average number of charges per droplet. These simultaneous increases make it possible that the N/N_0 ratio (see eq. 4) does not change nearly as fast as the ES current changes.

In considering the case of ubiquitin that has 76 amino acid residues (MQIFVKTLTG KTITLEVEPS DTIENVKAKI QDKEGIPPDQ QRLIFAGKQL EDGRTLSDYN IQKESTLHLV LRLRGG), with 12 of them being basic, when #2 µm and #5 µm tips are used, the N/N_0 values for 2 µM ubiquitin solution should be the same as 2 µM angiotensin solution, i.e., 130 and 49, respectively. The highest charge state observed in the mass spectrum was 10 for both spray tip sizes, and the ACS was 7.46 and 7.34, respectively (Fig. 8). Even when excess charges are plentiful, and even with larger spacing between basic residues, it appears to be more difficult to get larger peptides "fully" protonated than small peptides. This result is consistent with Downard and Biemann's finding[43] that charging did not increase proportionally with chain length for a series of peptides with a constantly repeating primary structure.

In further rationalizing the incomplete charging at higher **ESC** values, it is also likely that as the high voltage is increased, side reactions other than the production of H^+ become more favorable, and take on increasing importance. These secondary reactions can include oxidation of the tip itself, or the oxidation of impurities and/or other constituents in the solution. Even though the ES current may increase substantially, the number of excess protons that can attach to a peptide or protein is not likely to increase proportionally.

Conclusions

This investigation has explored how the spray tip orifice diameter affects the charge state distribution of selected peptides and a protein in nanoelectrospray. We focused on the responses of different diameter tips as the analyte concentration, buffer, and flow rate were directly varied, and on the indirect alteration of the number of excess charges. The changes pertaining to the **ACS** of angiotensin I in response to these variables are summarized in Table 2. From this table, it is clear that tips with *larger orifices* (e.g. 5 μm) are most susceptible to fluctuations in **ACS** due to changes in analyte concentration and initial solution pH, and are least affected by flow rate changes. For the tips with very *small orifices* (around 1 μm), the trend is the opposite, i.e, the flow rate affects the charge state distribution the most, while analyte concentration and the pH exhibit only very subtle effects. In all cases, the effect of augmenting the number of excess charges, by raising the applied high voltage and thus increasing ES current, is quite small. This is rationalized by considering that upon these changes, the flow rate will also increase. The additional charges available are thus counterbalanced by the increase in the number of

molecules present, hence the average charge state does not change significantly. If the analyst seeks to raise the number of charges imparted to a peptide (e.g., to achieve more reactive precursors for tandem mass spectrometry experiments), then the use of narrow diameter capillaries is recommended. However, if one wants to promote the production of lower charge state ions (perhaps even singly charged for easier interpretation of product ion spectra from small molecule precursors), then wider diameter capillaries are suggested.

Acknowledgement

Financial support for this research was provided by the National Science Foundation through grant #CHE-9981948.

CHAPTER 3

Hydrophobic Component in Non-covalent Binding of Fusion peptides to Lipids as Observed by Electrospray Mass Spectrometry

Yan Li[1], Frederic Heitz[2], Christian Le Grimellec[3], and Richard B. Cole1,*

[1]Dept. of Chemistry, University of New Orleans, New Orleans, LA, USA 70148; [2]CRBM, CNRS-FRE 2593, Montpellier, France 34293; [3] C.B.S. INSERM U554, Montpellier Cedex, France 34090
*author to whom correspondence should be addressed

The fusion of a viral membrane with the host cell membrane, which is facilitated by viral envelope glycoproteins called fusion proteins, is critical to infection by viruses such as HIV and influenza. Fusion peptides correspond to short regions, rich in hydrophobic residues, within the ectodomain of these proteins, which can initiate membrane fusion by leading insertion into the host cell membrane[83-85]. A new strategy in HIV-1 therapy is to try to interrupt viral membrane fusion[1]. Of course, the success of this approach requires a detailed knowledge of the fusion mechanism, and investigation of interactions between fusion peptides and lipid bilayers is essential for improving the understanding of this process. In addition, when associated with a polar nuclear localization sequence (NLS), thus offering amphipathic character, fusion peptides can act as efficient drug carriers by facilitating drug insertion and translocation across the cellular membrane[86]. It has been shown by a variety of methods that hydrophobic interactions, electrostatic interactions and conformational changes of both the peptide and the membrane all contribute to the transfer of the peptide from the aqueous phase through the lipid membrane[87-90].

One advantage of using electrospray mass spectrometry (ES-MS) to study the interactions of biomolecules is that non-covalent associations that exist in solution can survive the transfer into the gas phase[91-93]. However, studies have shown that gas-phase noncovalent adduct ions observed by mass spectrometry may or may not reflect the status of the component molecules in solution[94-98]. Up until now, a moderate noncovalent binding strength was considered to be essential to allowing observation of intact complexes, and it has been established that upon transfer to the gas-phase, electrostatic interactions are strengthened, while hydrophobic interactions are weakened[93].

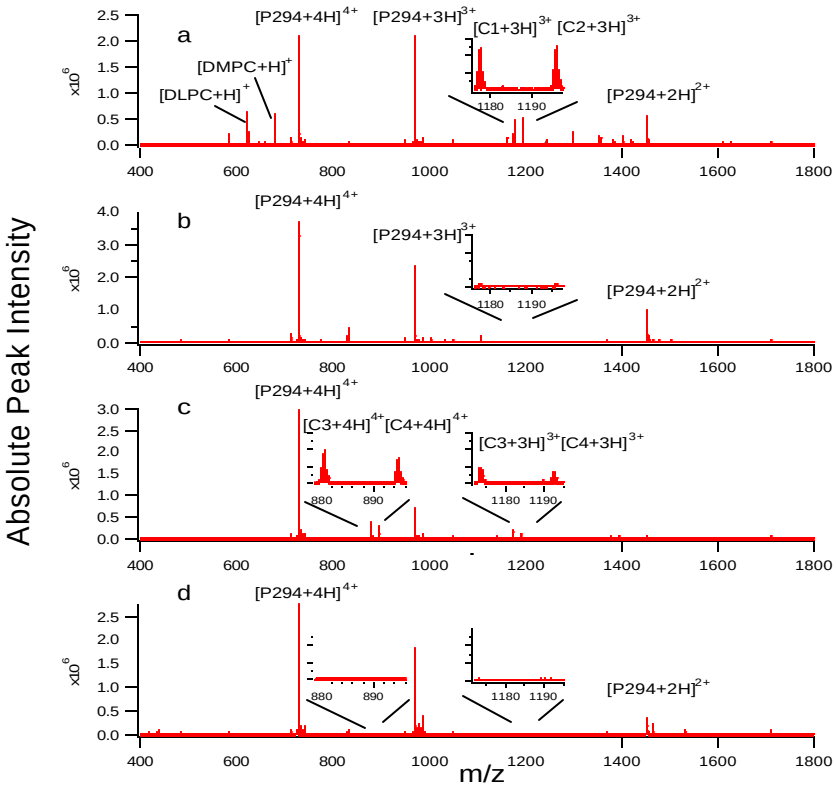

Fig. 1. Electrospray mass spectra of (1:1:1): (a) P294:DLPC:DMPC aqueous solution; (b) P294:DLPC:DMPC in methanol:water (30:70); (c) P294:DLPG:DMPG aqueous solution; (d) P294:DLPG:DMPG in methanol:water (30:70). C1, C2, C3, and C4 represent the triply charged (1:1) [P294+DLPC], [P294+DMPC], [P294+DLPG], and [P294+DMPG] complexes, respectively.

Noncovalent lipid-peptide or lipid-protein interactions are characterized by both electrostatic and hydrophobic components. Reports of the use of mass spectrometry to observe noncovalent complexes between lipids and proteins (soluble[99] or membrane[100]) have appeared only very recently. Our initial efforts[101,102] differ from those reports because we specifically probe the hydrophobic aspect of initial binding, and we target lipid interactions with peptides. In the current study, nanoelectrospray-FTICR was employed to investigate binding specificities of selected phosphatidylcholines (PCs) and phosphatidylglycerols (PGs) with the fusion peptide P294 (Ac-GALFL GFLGA AGSTM GAWSQ PKKKR KV-Cya, where Ac = CH_3CO and Cya = NH-CH_2-CH_2-SH). The ratio of (total complexed)/(total unbound) peptide was used to evaluate the relative binding strengths of lipid-peptide complexes.

In positive ion mass spectrometry experiments performed on a Bruker Apex II 7.0 Tesla FT-ICR, the dominant complexes detected under a variety of conditions were (1:1) P294:lipid complexes. The phopshatidylglycerols (PG) (dilauryl = DLPG and dimyristyl = DMPG, Fig. 1c) generally showed stronger binding affinities for P294 than the phosphatidylcholines (PC) (DLPC and DMPC, Fig. 1a). The zwitterionic PC head groups are overall neutral, whereas PGs are negatively charged. The fact that DLPG and DMPG bind more tightly with P294 than DLPC and DMPC, respectively, shows the significance of the electrostatic interaction in stabilizing peptide-lipid complexes. Also worth noting is that a phosphatidylcholine with one unsaturation on each acyl chain (i.e., 14:1 PC) exhibited a binding affinity with P294 that was quite similar to that of DMPC (14:0 PC).

To shed light upon whether the detected complexes are representative of solution phase complexes, as opposed to being formed in the gas phase (i.e., by a drawing together of

the constituent molecules as the last solvent molecules from the final ES droplets evaporate), mixtures identical to those above made in pure water were remade in 30:70 methanol:water. Increasing volume fractions of methanol in aqueous systems have been shown to weaken the hydrophobic interaction between peptides and nonpolar stationary phase particles as manifested by steady decreases in the capacity factor in reversed-phase liquid chromatography experiments[103]. Addition of 30% methanol resulted in no detectable binding between P294 and either DLPC or DMPC (Fig. 1b). Similar results were obtained for the equimolar DLPG and DMPG solution containing P294 when the solvent was changed to 30:70 methanol:water (Fig. 1d). These results strongly suggest that the ES-MS detected [DLPC + P294], [DMPC + P294], [DLPG + P294] and [DMPG + P294] complexes were already formed in solution, with the hydrophobic effect being the primary driving force promoting the interaction. If gas-phase processes (i.e., increased electrostatic attraction at the moment when the final solvent molecules depart) rather than hydrophobic interaction (in the initial solution) were responsible for enabling detection of these complexes, the improved desolvation conditions of 30:70 methanol relative to pure water would not be expected to disrupt binding.

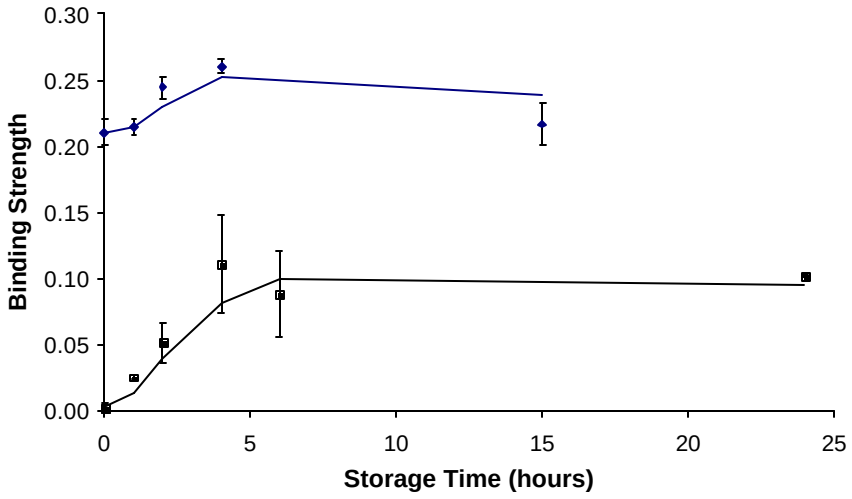

Fig. 2. The binding strength of the [P294+DMPG] complex (top) was much larger than that of the [P294+DMPC] complex (bottom). Upon storage at 0 °C for intervals of up to ~4 hours, the signal of the detected [P294+DMPC] complex increased steadily, while the binding between P294 and DMPG was also strengthened, but to a less obvious extent.

The binding between P294 and DMPC was barely detectable just after vortex of the aqueous solution. But upon storage at 0 °C for intervals of up to 4 hours, the signal of the detected [P294+DMPC] complex increased steadily (Fig. 2). Apparently, these molecules in aqueous solution required some time to orient themselves into low-energy conformations. Moreover, lower temperatures favored formation of weak complexes. As shown in Fig 2, DMPC (zwitterionic head group) required significantly longer time intervals to form complexes than DMPG (anionic head group). This result, combined with the overall weaker binding of DMPC vs. DMPG is consistent with the interpretation that hydrophobic interactions play a key role in forming [P294+DMPC] solution phase complexes.

To test the influence of solution conductivity on lipid-peptide binding, aqueous ammonium acetate solutions (hereafter referred to as “buffered” solutions) of varying concentration were employed in preparing (1:1:1) P294:DLPC:DMPC mixtures. Fig. 3 shows that the [peptide+lipid] binding strength, as expressed by the quotient of (total observed [P294+lipid] complexes)/(total free P294), increased as the buffer concentration was raised from 0 to 200 μM. This strengthened interaction is rationalized based upon an increased *hydrophobic* effect at raised ionic strengths. If hydrophobic interactions were paramount for complex formation, one might expect the binding strength to increase as a function of the ionic strength of the solution. Notably, however, further increase of the buffer concentration (to 400 μM and beyond) caused the [peptide+lipid] binding strength to decrease. It is likely that raising the ionic strength of the solution had a secondary effect of increasing solvation of the charge sites on both peptide and lipid, thus weakening the *electrostatic* interaction. The peak maximum in Fig. 3 likely corresponds

to the most favorable balance between the augmented, but leveling, hydrophobic effect, and the continually diminishing electrostatic component.

In considering the structures of the employed phosphatidylcholines, each of the two tail chains of DMPC has an additional $-CH_2CH_2-$ unit relative to those of DLPC. In neat or buffered aqueous solutions, 20-200 μM DMPC and DLPC will each have bilayer (rather than micellar) conformations[104], and they generally exhibited almost the same binding affinities for P294 (Fig. 3). However, as the ionic strength of the solution was increased, the binding strength of the [P294+DMPC] complex became noticeably higher than that of the [P294+DLPC] complex. This behavior can be rationalized by considering that a stronger degree of hydrophobic interaction exists between P294 and DMPC owing to an increased nonpolar interaction for the longer hydrocarbon chain. As the buffer concentration becomes significant, the subtle difference in the magnitude of the hydrophobic effect becomes more pronounced.

To further examine the contribution of the hydrophobic interaction to lipid-peptide binding, experiments were performed using a peptide of known hydrophilic character, i.e., Fibrinopeptide B. A (1:1) fibrinopeptide B:DMPG mixture showed moderate binding between fibrinopeptide B and DMPG in pure aqueous solution, that was rather unperturbed by the addition of 30% methanol. This result presents a sharp contrast to that depicted in Figs. 1c and 1d for the [P294+DMPG] complex, and offers additional evidence that hydrophobic forces play a key role in the mass spectrometrically observed binding between the fusion peptide P294 and DMPG.

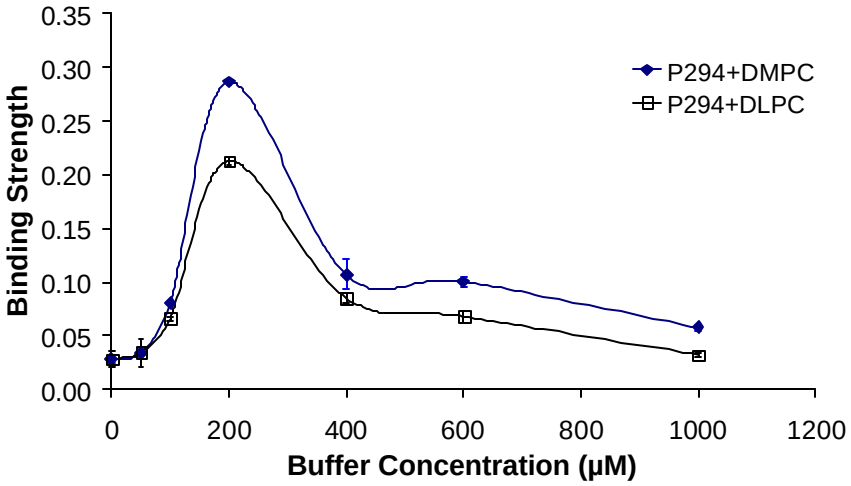

Fig. 3. The binding strength of [P294+DMPC] (solid triangles, upper trace) and [P294+DLPC] (hollow squares, lower trace) complexes as a function of buffer concentration.

Although their binding strengths are likely altered by increased electrostatic interactions in the gas phase, compiled evidence shows that the [P294+PC] and [P294+PG] complexes detected by ES-MS already existed in solution. Evidence further indicates that initial hydrophobic interactions in solution contributed heavily to the formation of these peptide-lipid complexes, particularly for [P294+PC] complexes, while electrostatic interactions played a larger role for [P294+PG] complexes. The ability to observe noncovalent interactions driven primarily by hydrophobic interactions is a new capability that will find utility in better defining interactions between fusion peptides and lipid components in cell membranes, as is currently underway in our laboratory. These experiments help to establish ES-MS as a viable new biotechnology tool capable of providing valuable information regarding the strength of hydrophobically driven, noncovalent interactions.

Acknowledgments: Partial support for this research was provided by the U.S. Dept. of Energy through grant number DE-FG02-02ER63378 (YL and RBC), and by EU grant QLK2-2001-01451 (FH and CLG).

CHAPTER 4

Lipid-Peptide Non-covalent Interactions Observed by Nano-electrospray FT-ICR

Yan Li[1], Frederic Heitz[2], Christian Le Grimellec[3], and Richard B. Cole[1,*]

[1]Dept. of Chemistry, University of New Orleans, New Orleans, LA, USA (70148; [2]CRBM, CNRS-FRE 2593, Montpellier, France 34293; [3] C.B.S. INSERM U554, Montpellier Cedex, France 34090

**author to whom correspondence should be addressed*

Introduction

The fusion of a viral membrane with the host cell membrane is an important step in infection by viruses such as HIV and influenza. This membrane fusion process is facilitated by viral envelope glycoproteins called fusion proteins. Investigations into ways to block viral membrane fusion are now being pursued as means to combat the spread of disease(1), which requires a detailed knowledge of the fusion mechanism. Fusion peptides correspond to short regions, rich in hydrophobic residues, within the ectodomain of these proteins, which can initiate membrane fusion by leading insertion into the host cell membrane[83-85]. It is believed that fusion peptides exist as a central motif in the mechanism of fusion in all viral membrane proteins[122]. Investigation of interactions between fusion peptides and lipid bilayers is essential for improving the understanding of the membrane fusion process. In addition, when associated with a polar nuclear localization sequence (NLS) that targets the cell nucleus, thus offering amphipathic character to the molecule, fusion peptides can act as efficient cargo carriers by facilitating transport and passage across the cellular membrane[86].

It has been shown by a variety of methods that hydrophobic interactions, electrostatic interactions and conformational changes of both the peptide and the membrane all contribute to the translocation of the peptide from the aqueous phase through the lipid membrane[87-90]. However, reports of the use of mass spectrometry to observe noncovalent complexes between lipids and soluble proteins[99], membrane proteins[100] or peptides[102] have appeared only very recently.

Compared to older mass spectrometric ionization techniques, electrospray mass spectrometry (ES-MS) has the advantage of enabling the preservation of non-covalent

associations that exist in solution[91-93]. However, there is often concern that the gas-phase ions representing noncovalent complexes observed by mass spectrometry may not reflect the status of the component molecules in solution[94-98]. Moreover, it has been established that as evaporation of solvent molecules in the final charged electrospray droplets proceeds, electrostatic interactions are strengthened, while hydrophobic interactions are weakened[93].

In biological systems, noncovalent lipid-peptide or lipid-protein interactions are characterized by both electrostatic and hydrophobic components. Our initial efforts[102] specifically targeted the hydrophobic aspect of initial binding between lipids and peptides. In the current study, we broaden and deepen our investigations into the detailed binding specificities between selected phospholipids and model fusion peptides.

Experimental Section

Sample preparation

Selected phosphatidylcholines (PCs) and phosphatidylglycerols (PGs) were purchased from Avanti Polar Lipids (Alabaster, AL) without further purification. Fusion peptide P294 (Ac-GALFL GFLGA AGSTM GAWSQ PKKKR KV-Cya,) and P326 (Ac-GALFL AFLAA ALSLM GLWSQ PKKKRKV-Cya where Ac = CH_3CO and Cya = NH-CH_2-CH_2-SH) were synthesized by the laboratory of Frederic Heitz in Montpellier, France.

200 μM fusion peptides stock solutions were prepared in methanol, then immediately divided into several portions, followed by removal of methanol. The dried peptides were stored at -80 ºC. For each set of comparison experiments, solutions of the same fusion peptides were made from the same sample batch. The stock solutions of lipids were made

to 2.0 mM in chloroform and stored at -80 ºC for no longer than 10 days. For each set of comparison experiments, solutions of the same lipid were made from the same batch of stock solution.

The aqueous solutions containing peptide(s) + lipid(s) mixtures were made in three steps. First, delivering a certain volume of lipid(s) stock solution(s) into a vial, and removing the chloroform by vacuum centrifuge, followed by dry N_2 steam for about 2 min; Second, dissolving the fusion peptide(s) in pure water to a certain concentration, then combining with the lipid(s) to the desired concentrations; Third, vortex the solution mixture at room temperature for 1 hour.

We already reported[102] that the binding between P294 and DMPC was barely detectable just after vortex of the aqueous solution, but upon storage at 0 °C for intervals of up to 4 hours, the signal of the detected [P294+DMPC] complex increased steadily. It seems these molecules in aqueous solution required some time to orient themselves into low-energy conformations. The fact that DMPC required significantly longer time intervals to form complexes than DMPG, combined with the overall weaker binding of DMPC vs. DMPG is consistent with the interpretation that hydrophobic interactions play a key role in forming [P294+DMPC] solution phase complexes. In this study, spectra were obtained after the peptide(s) + lipid(s) mixture solutions were stored at 0 °C for 4 to 6 hours.

Mass spectrometry

All experiments were performed in the positive mode on a Bruker (Billerica, MA) 7.0 T Fourier transform ion cyclotron resonance mass spectrometer (FT-ICR-MS). In order to

obtain a balance between a stable strong signal and maintaining "soft" ES conditions, voltages on the capillary exit and the skimmer were fixed at 40 and 12 volts, respectively. Electrospray current was maintained at 10-20 nA for most experiments.

Nanospray tips were purchased from New Objective (Woburn, MA). The ID of intact tips were marked as 1 μm. To reduce clogging, nanospray tips were broken to widen the aperture; the ID of broken tips were measured and estimated to be approximately 10 μm.

For each solution, at least three spectra were acquired under the same conditions. Each new spectrum was obtained after turning off, then on, the high voltage. The ratio of (total complexed)/(total unbound) peptide was used to evaluate the relative binding strengths of lipid-peptide complexes. For all presented plots, each point represents the average of at least three measurements, and error bars show the standard deviations of the three measurements.

Results and Discussion

Lipid bilayers

As the volume of a micelle increases, the surface/volume ratio always decreases[104]. The repulsive force coming primarily from similarly charged head groups increases as the area per head group decreases. Thus, for a stable micelle, there is an optimal area per head group. Model phospholipids employed in this study have two hydrocarbon tails, thus the area per head group is about twice as large as those with one tail. The employed phospholipids tend to form large disklike bilayer micelles in aqueous solution[104]. It has been reported that the CMC of didecanoyl phosphatidylcholine and dipalmitoyl phosphatidylcholine are 5×10^{-6} M[123] and 4.7×10^{-10} M[124], respectively. It is estimated that

the CMC decreases by about 10-fold when the hydrocarbon chain length increases by a CH_2CH_2 unit[104]. A typical lipid concentration employed in this experiment is 20 μM. At this concentration, DLPC (1,2-Dilauroyl-sn-Glycero-3-Phosphocholine) and DMPC (1,2-Dimyristoyl-sn-Glycero-3-Phosphocholine) form bilayers in aqueous solution.

There was no directly related CMC data found for phosphatidylglycerol employed in this experiment. However, King et al showed that CMC value of PG is about 1.7 times higher than that of PC with the same tail chain length[125]. Based on this estimation, DLPG (1,2-Dilauroyl-sn-Glycero-3-[Phospho-rac-(1-glycerol)]) and DMPG (1,2-Dimyristoyl-sn-Glycero-3-[Phospho-rac-(1-glycerol)]) employed in this study also form bilayers in aqueous solution.

Origin of error

1. Lipids have different ionization efficiencies

It has been shown that the type of head group, acyl chain length and the degree of unsaturation all affect the mass spectrometric response of lipids[126]. The electrospray ionization efficiencies of both saturated and unsaturated phospholipids decreased with increasing chain length[126]. For phosphatidylchilone, as the chain length increased from 12 to 24, the ES ionization efficiency decreased linearly at low concentration (0.2 μM) and had an exponential decay at high concentration (10μM)[127].

Because of the weak nature of the non-covalent binding between fusion peptides and lipids, a high lipid concentration (typically 20 μM) is required to mass spectrometrically detect binding. Although the chain length of naturally occur lipids is usually equal to or larger than 12 carbon atoms, limited by the non-negligible difference between their

ionization efficiencies, DLPC/DMPC and DLPG/DMPG were chosen as model lipids to study the effect of chain length on peptide-lipid binding. Potential problems are that it is hard to evaluate the reproducibility of the lipid concentrations (or their ratio) from batch to batch; and some differences in the ionization efficiencies of the complexes are expected.

The magnitude of hydrophobic interaction is weakened by the presence of double bonds in the lipids' tail chains[104]. It was noted that the ionization efficiency of unsaturated phospholipids was significantly increased relative to their saturated counterparts[126]. So PCs with tail chain lengths up to 18 carbon atoms were employed: 1,2-Dimyristoleoyl-sn-Glycero-3-Phosphocholine, 1,2-Dioleoyl-sn-Glycero-3-phosphocholine and 1,2-Dilinolenoyl-sn-Glycero-3-Phosphocholine, simplified as (14:1)PC, (18:1)PC and (18:3)PC, respectively.

2. Lipids could be in different phase state

At temperatures lower than the transition temperature (Tm), the lipid molecules yield more orderly arrays and form a gel-like solid. Above the Tm, called a liquid crystal state, the hydrophobic core of the bilayer can be treated as a hydrocarbon liquid because lipid molecules are highly mobile[104]. Studies have shown that the nature of the lipid phase can significantly affect the peptide/protein-lipid binding[128-131]. In many cases, peptides were found to associate more strongly with bilayers in the liquid crystal state[128,130,131]. However, in some studies, peptides displayed a stronger interaction with membranes in the gel-solid phase[129].

We have shown that binding between P294 and DMPC steadily increased upon storage at 0 ºC for up to 4 hours. That does not necessarily mean that P294 binds stronger to gel-solid state DMPC. In our studies, we mixed the peptide and lipid in aqueous solution at room temperature for 1 hour before storing the solution at 0 °C for 4 to 6 hours. Table 1 lists the model compounds employed in this study and their Tm's. DLPC and DLPG are in the liquid crystal phase during mixing or upon storage at 0 °C, whereas DMPC and DMPG are in gel-solid state during storage at 0 °C. This could introduce a potential problem when comparing the binding strengths of complexes formed by peptides with DLPC/DLPG as opposed to those formed with DMPC/DMPG. However, studies have shown that adding in peptide could change the Tm of the lipid[131-133], commonly increasing the Tm when the peptide penetrates deep into the hydrophobic core[132]. So it is possible that with the addition of P294/P326, DLPC and DLPG are also in the gel-solid state upon storage at 0 °C.

Table 1. Model lipids and their transition temperatures

lipid	DLPC	DMPC	(14:1)PC	(18:1)PC	(18:3)PC	DLPG	DMPG
Tm (ºC)	-1	23	<-20[a]	-20	-60	-3	23

PC vs. PG

The dominant complexes detected under a variety of conditions were (1:1) P294:lipid complexes. It has been noted that the phopshatidylglycerols (PG) generally showed stronger binding affinities for P294 than the phosphatidylcholines (PC) by comparing the binding strengths of corresponding complexes in P294+PC mixtures with those of separate P294+PG mixtures[102]. In a more direct comparison, from the spectrum obtained

from a P294:DMPC:DMPG = 20:20:20 μM aqueous solution (Fig. 1) where competition for peptide binding between DMPC and DMPG can be directly probed, the binding strength of [P294+DMPG] complexes was clearly higher than that of [P294+DMPC] complexes. The zwitterionic PC head groups are overall neutral, whereas PGs are negatively charged. Thus, the increased electrostatic interaction between PG and positively charged peptide must play a significant role in stabilizing peptide-PG complexes.

Fusion peptide P326

Table 2 summarizes the sequence difference between P326 (Ac-GALFL AFLAA ALSLM GLWSQ PKKKRKV-Cya, where Ac = CH_3CO and Cya = NH-CH_2-CH_2-SH, Mr = 3044.7548) and P294 (Ac-GALFL GFLGA AGSTM GAWSQ PKKKR KV-Cya, Mr = 2906.5775).

Residues where difference occur	6	9	12	14	17
P294	G	G	G	T	A
P326	A	A	L	L	L

The order of side-chain length is glycine (G) < alanine (A) < leucine (L). Also theronine (T) is polar while leucine is nonpolar. So generally, several nonpolar residues with shorter side chains in P294 were replaced by those with longer side chains and one polar residue in P294 was substituted by nonpolar leucine.

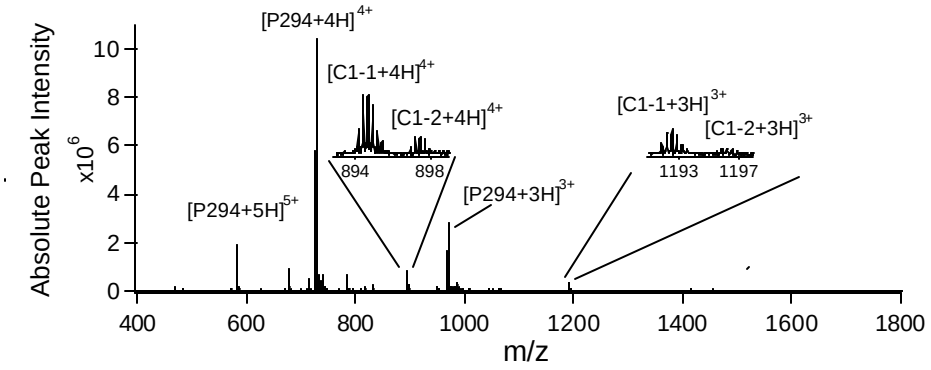

Fig. 1. Electrospray mass spectrum of (20:20:20 μM) P294:DMPC:DMPG aqueous solution. "C1-1" and "C1-2" represent [P294+DMPG-Na+H] and [P294+DMPC] complexes, respectively.

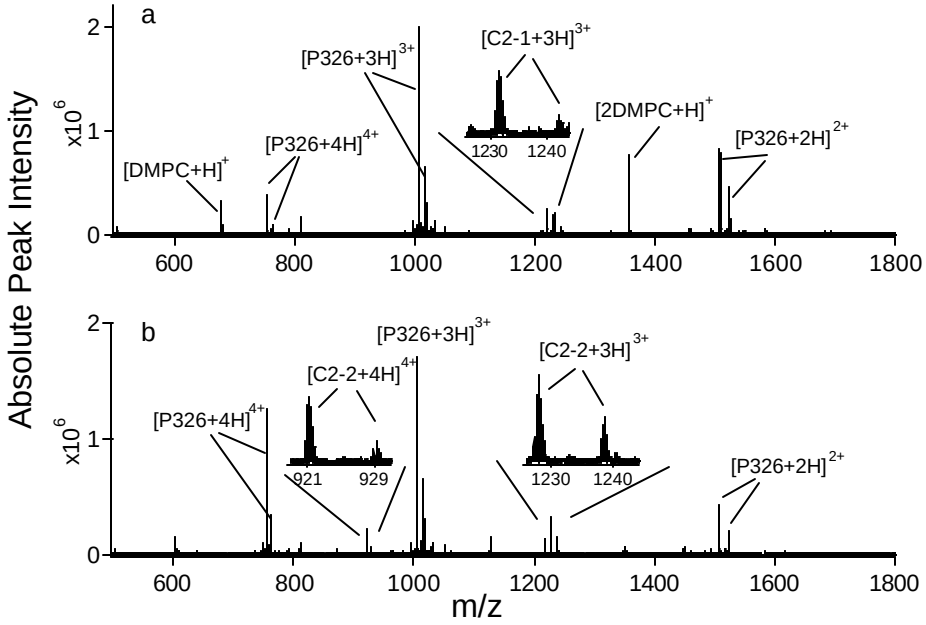

Fig. 2. Electrospray mass spectra of (a) P326:DMPC (20:20 μM) aqueous solution; and (b) P326:DMPG (20:20 μM) aqueous solution. Peaks represent both "P326" and "P326-S" were marked as "P326". Their corresponding complexes were marked as "P326 complex". "P326-S" and "P326" showed similar binding strength to both PC and PG. "C2-1" and "C2-2" represent [P326+DMPG-Na+H] and [P294+DMPC] complexes, respectively.

CD studies showed that P294 is a random coil in water and in a ß-sheet conformation in lipid; while P326 is in a a-helix conformation both in water and in lipid.

Like P294, P326 showed affinity to both PC (Fig. 2a) and PG (Fig. 2b), although, as was the case for P294, PG binds more tightly with P326 than PC. It is again clear that the electrostatic interactions contributed more heavily to the binding between fusion peptides and PG as compared to PC. It must be mentioned that, in addition to the peaks corresponding to intact P326 (Mr = 3044.75), there were peaks of even higher abundance corresponding to a single impurity whose Mr = 3012.68. From the results of an MS/MS/MS study and information concerning the synthesis process, we were able to unequivocally assign this impurity as an analog P326 with a C-terminus of -NH-CH_2-CH_3 instead of -NH-CH_2-CH_2-SH. Binding strength calculations on 5 spectra showed that (1:1) [P326-S+DMPC] complexes had binding strengths that were virtually identical to those of (1:1) [P326+DMPC] complexes (0.09 ± 0.01 for [P326-S+DMPC] complexes, 0.08 ± 0.01 for [P326+DMPC] complexes) obtained in the same spectrum. Calculated in the same way, the binding strength for [P326-S+DMPG] and [P326+DMPG] were 0.15 ± 0.01 and 0.16 ± 0.02, respectively. Because peptide “P326-S” and its complexes had higher peak intensities than those of P326, we considered them to be more reliable, hence, they were used in subsequent calculations of the binding strengths of P326+lipid complexes.

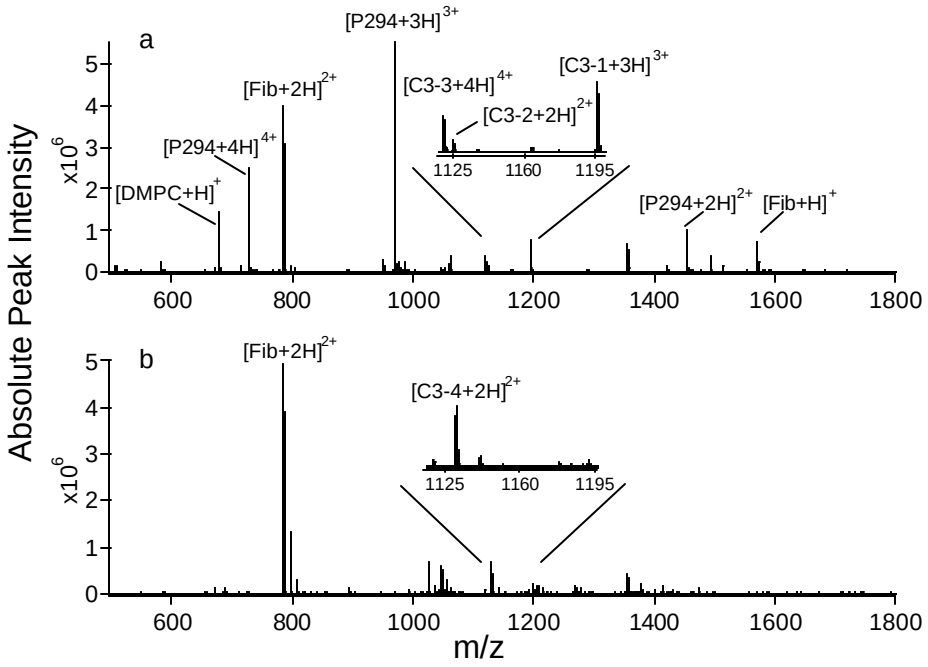

Fig. 3. Electrospray mass spectra of (a) P294:Fib-B:DMPC (20:20:20 µM) aqueous solution; and (b) P294:Fib-B:DMPG (20:20:20 µM) aqueous solution. In 3a, "C3-1", "C3-2", and "C3-3" represent [P294+DMPC], [Fib-B+DMPC] and [P294+Fib-B] complexes, respectively. In 3b, "C3-4" represents [Fib-B+DMPG] complex.

Fusion peptides vs. hydrophilic peptide

Fibrinopeptide B (EGVNDNEEGFFSAR, Mr = 1569.6695) (simplified as Fib-B) is a peptide with obvious hydrophilic character. To further examine the contribution of the hydrophobic interaction to lipid-peptide binding, experiments were performed using equimolar concentrations of P294 and Fib-B competitively binding to DMPC (Fig. 3a) and DMPG (Fig. 3b). In the spectrum obtained from a P294:Fib-B:DMPC = 20:20:40 μM aqueous solution (Fig. 3a), the main bound complexes detected were: $[P294+DMPC+3H]^{3+}$ (m/z = 1195.7), $[P294+Fib\text{-}B+4H]^{4+}$ (m/z = 1119.9), $[P294+Fib\text{-}B+4H]^{3+}$ (m/z = 1492.8). The peak corresponding to $[Fib+DMPC]^{2+}$ (m/z = 1124.4) was very weak and not stable, and in some spectra, it was not even visible above the noise. The order of absolute peak intensity is [P294+DMPC] > [P294+Fib-B] >> [Fib-B+DMPC]. That means in this condition ([Fib-b] = 20 μM, [DMPC] = 40 μM) , P294 binds more strongly to DMPC than to Fib-B, whereas under same condition, Fib-B binds more strongly to P294 than to DMPC. By comparing the value of the calculated binding strength of [P294+DMPC] (0.12 ± 0.02) and [Fib-B+DMPC] (0.04 ± 0.04), it is clear that the fusion peptide binds more strongly to DMPC than does the hydrophilic peptide Fib-B. This result offers further evidence that hydrophobic interactions play a key role in the binding between fusion peptide and PC.

In the spectrum obtained from a P294:Fib-B:DMPG = 20:20:40 μM solution (Fig. 3b), the dominant peak was $[Fib\text{-}B+2H]^{2+}$ (m/z = 785.8). $[Fib\text{-}B+DMPG+3H\text{-}Na]^{2+}$ (m/z = 1118.9) showed moderate binding strength, whereas neither unbound P294 nor [P294+DMPG] complexes showed detectable peaks. Because PG is negatively charged in the solution, these results can be explained by considering that electrostatic interactions

contributed most heavily to the binding which brought Fib-B and DMPG together. While signals for P294 and its complexes were suppressed in the P294:Fib-B:DMPG (20:20:40 μM) aqueous solution, P294 showed strong signal in both P294:Fib-B (20:20 μM) and P294:DMPG (20:20 μM) aqueous mixtures.

Effects of methanol addition

It has been shown by HPLC studies that an increase in the methanol volume weakens the hydrophobic interactions between the C18 stationary phase and the analytes[103]. Methanol addition can thus be considered as a means to disfavor hydrophobic interactions in aqueous systems. Five kinds of peptide-lipid combinations with fixed peptide:lipid concentration ratio were tested in this set of experiments. Fig. 4 showed the response of each combination to the addition of methanol.

In a P294:DLPC:DMPC = 20:20:20 μM solution (Fig. 4a), increasing the methanol volume fraction to 0.20 totally destroyed the binding between P294 and DLPC/DMPC. A further increase in the methanol volume fraction to 0.30 also resulted in no binding detected. The fact that the binding between P294 and PC was destroyed by addition of 20% methanol offered further evidence that the [P294+PC] complexes were already formed in the 100% aqueous solution, with the hydrophobic interactions as the primary driving force promoting the interaction. If gas-phase processes (i.e., increased electrostatic attraction at the moment when the final solvent molecules depart) rather than hydrophobic interaction (in the initial solution) were responsible for enabling detection of

these complexes, the improved desolvation conditions (because of methanol addition) would not be expected to disrupt binding.

For a P326:DLPC:DMPC = 20:20:20 μM solution (Fig. 4b), the binding strength of [P326+PC] complexes in 100% aqueous solution was stronger as compared to [P294+PC] complexes (Fig. 4a). Higher methanol volume fraction (~0.37) was needed to diminish the binding to zero (for DLPC) or near zero (for DMPC). Further increases in the methanol volume fraction resulted in the re-appearance of binding for [P326+DLPC], and to a lesser degree, for the binding of [P326+DMPC]. It is reasonable that a higher percentage of methanol is needed to destroy stronger hydrophobic interactions. The re-appearance of binding could be due to an increased chance for electrostatic interactions to happen following faster solvent evaporation at higher methanol volume fraction. These interactions were likely of lower magnitude in the initial solution of no methanol content. The sites where electrostatic interactions happen will be the same for both DLPC and DMPC, but [P294+DLPC] complexes may be more sensitive to the electrostatic interactions.

When using PG instead of PC, i.e. in a P294:DLPG:DMPG = 20:20:20 μM solution (Fig. 4c), again a stronger binding was shown between P294/PG than P294/PC (Fig. 4a). The stronger binding for PG is attributed to a stronger electrostatic interaction. A higher methanol volume fraction (~0.31 for DLPG, ~0.33 for DMPG) was needed to weaken the binding strength of [P294+PG] complexes to zero relative to DLPC and DMPC complexes (~0.20 methanol volume fraction required for both). At even higher methanol percentages, both [P294+DLPG] and [P294+DMPG] complexes re-appeared with the binding strength of the former rising more steeply than that of the latter (Fig. 4c). PG is

negatively charged in the solution. This re-appearance of the complexes may also be explained by considering that in solvents of higher methanol content (e.g. 50%), desolvation is improved so substantially that electrostatic interactions become dominant between the species present in the final droplets.

For a P326:DLPG:DMPG = 20:20:20 μM solution (Fig. 4d), in 100% aqueous solution, again PG bound more strongly to P326 than PC (Fig. 4b). In addition, the signal of the complexes diminished to zero (for DMPG) or near zero (for DLPG) by a higher methanol volume fraction (~0.41); again upon further increasing the methanol portion the complexes reappeared, with the binding strength of detected [P326+DLPG] complexes rising faster than that of [P326+DMPG] complexes.

A sharp contrast could be seen when checking the response of the detected binding between the hydrophilic peptide Fib-B and DMPG upon addition of methanol (Fig. 4e). As the methanol volume fraction increased, after a small initial decrease, the detected binding strength eventually increased. This contrasting result from a hydrophilic peptide that showed only a minor decrease in binding to lipids upon initial addition of methanol, offers additional evidence that hydrophobic forces play a key role in the mass spectrometrically observed binding between the fusion peptide P294 and DMPG.

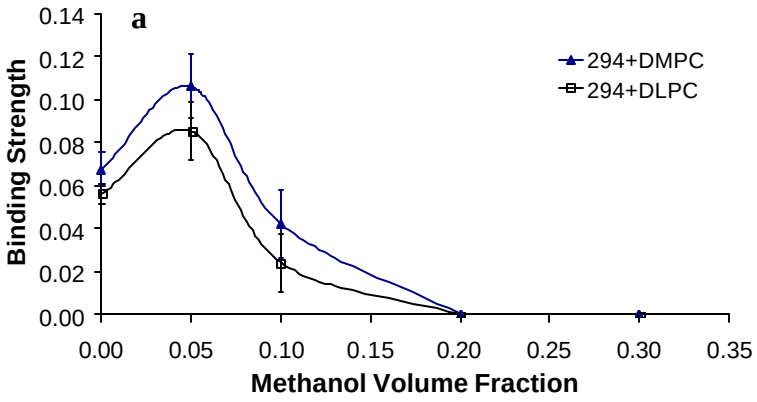
a
294+DMPC
294+DLPC
Binding Strength
0.14
0.12
0.10
0.08
0.06
0.04
0.02
0.00
0.00 0.05 0.10 0.15 0.20 0.25 0.30 0.35
Methanol Volume Fraction

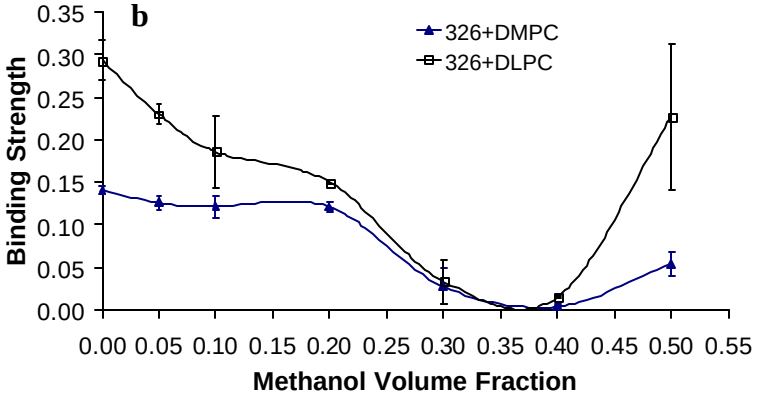
b
326+DMPC
326+DLPC
Binding Strength
0.35
0.30
0.25
0.20
0.15
0.10
0.05
0.00
0.00 0.05 0.10 0.15 0.20 0.25 0.30 0.35 0.40 0.45 0.50 0.55
Methanol Volume Fraction

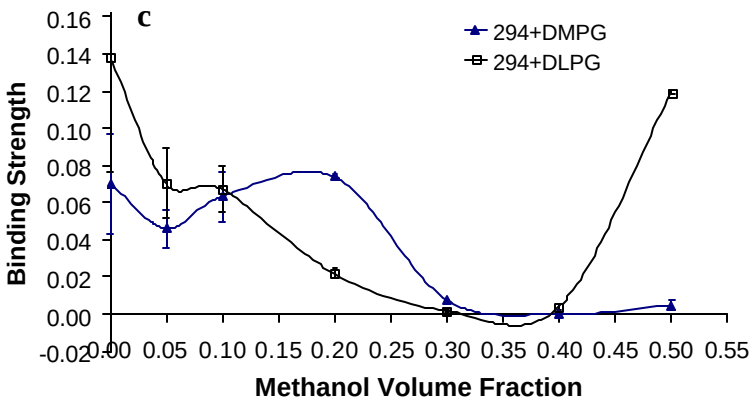
c
294+DMPG
294+DLPG
Binding Strength
0.16
0.14
0.12
0.10
0.08
0.06
0.04
0.02
0.00
-0.02
0.00 0.05 0.10 0.15 0.20 0.25 0.30 0.35 0.40 0.45 0.50 0.55
Methanol Volume Fraction

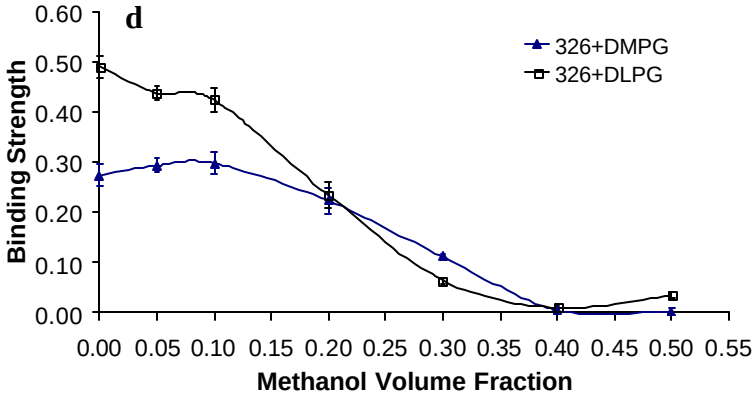
d
326+DMPG
326+DLPG
Binding Strength
0.60
0.50
0.40
0.30
0.20
0.10
0.00
0.00 0.05 0.10 0.15 0.20 0.25 0.30 0.35 0.40 0.45 0.50 0.55
Methanol Volume Fraction

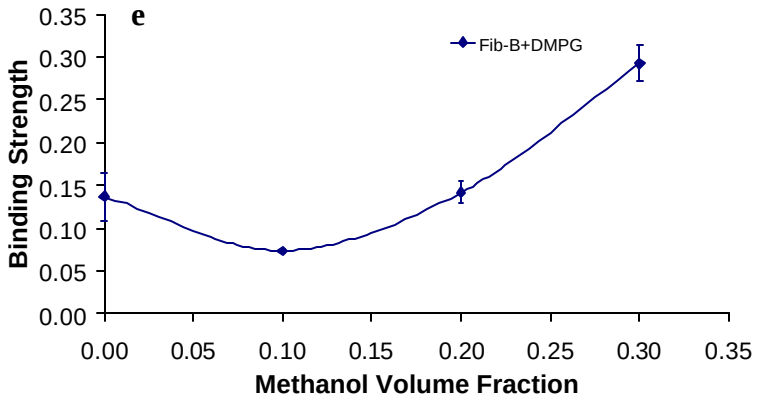

Fig. 4. The change of binding strength of [peptide+lipid] complexes in five peptide-lipid combination system as the addition of methanol.

4a) a P294:DLPC:DMPC = 20:20:20 μM solution;

4b) a P326:DLPC:DMPC = 20:20:20 μM solution;

4c) a P294:DLPG:DMPG = 20:20:20 μM solution;

4d) a P326:DLPG:DMPG = 20:20:20 μM solution;

4e) a Fib-B:DMPG = 20:20 μM solution

Binding at low pH

It has been reported that a fusion peptide found in the influenza virus' fusion protein, haemagglutinin, only interacted with the target membrane at low pH[122], whereas the fusion peptide of HIV viruses is active both at low and neutral pH[134]. In this experiment, "acidified solution" was obtained by adding acetic acid to pure aqueous solution. The pH of 0%, 0.01%, 0.05%, 0.1%, and 1% acetic acid solutions were 5.5, 3.7, 3.4, 3.2, and 2.8 respectively. P294 showed slightly higher affinity to PC at pH 3.7 in P294:DLPC:DMPC = 20:20:20 μM "acidified" solution. With a further lowering of the solution pH, the binding decreased gradually (Fig. 5a). If one considers that addition of acetic acid also increases the ionic strength of the solution, the ionic strengths of 0.01%, 0.05%, and 0.1% acetic acid aqueous solution were 1.8×10^{-4}, 4.0×10^{-4}, 5.6×10^{-4} M, respectively. The binding strength of the complex reached an optimum value when the ionic strength of the solution was around 200 μM also. On the other hand, at the same ionic strength value, peptide/lipid binding was weaker in acidified solution than in buffered solution[102].

As compared to P294, the binding between P326 and PC showed a much sharper immediate decrease once 0.01% acetic acid was added (Fig. 5b). Further decrease of the pH to 2.8 (1% acetic acid aqueous solution) caused only slight further weakening of the binding strength of [P326+PC] complexes. Even with the sharp initial decrease in binding strength compared to the neat solution, P326 still showed stronger affinity to PC than P294 over the entire range, $3.2 < pH < 5.5$.

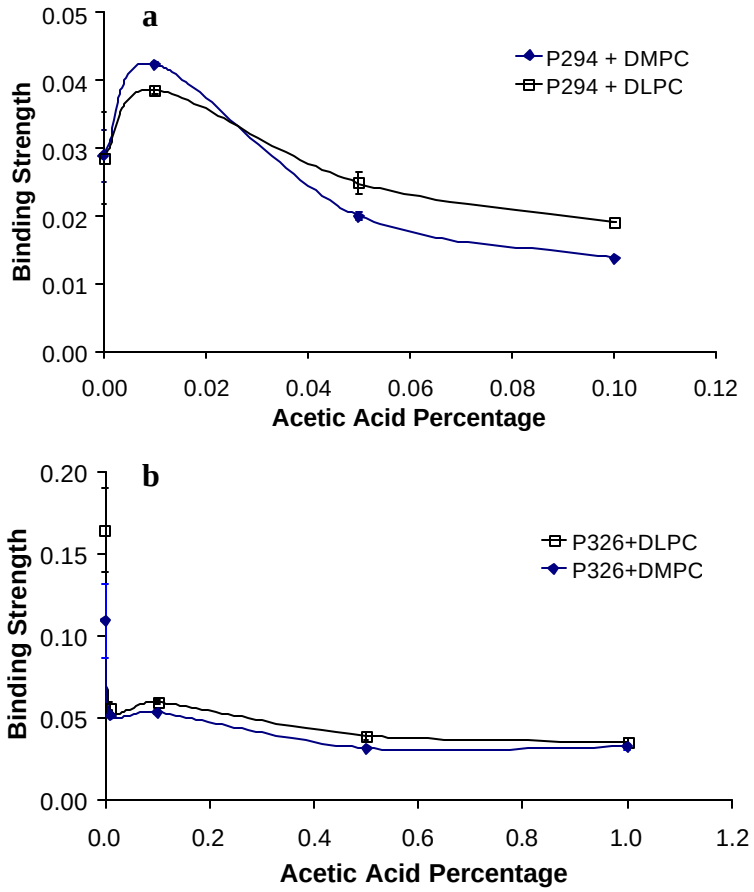

Fig 5. Binding between P294 and P326 with PC and PG at low pH. The calculation did not finish yet. Here just an example.
5a. P294:DLPC:DMPC = 20:20:20 μM
5b. P326:DLPC:DMPC = 20:20:20 μM

Binding to unsaturated PC

Unsaturated lipids are abundant in nature. More than half of plant and animal lipids are unsaturated and are often polyunsaturated. Double bonds in these lipids usually occur in the cis-configuration. It is important to test weather the model fusion peptides have affinity to unsaturated lipids as well. Since PC generally showed weaker binding to our model fusion peptides than PG, we choose to employ unsaturated PC to investigate the effects of lipids chain unsaturations. In this set of experiments, 1,2-Dimyristoleoyl-sn-Glycero-3-Phosphocholine (which has a 9-cis double bond on each tail chain, called (14:1)PC in this paper) was employed for a direct comparison with its saturated homolog, DMPC. Fig 6 shows that both P294 (6a) and P326 (6b) can each bind to unsaturated PC with approximately similar binding affinities as that of saturated PC of the same tail chain length. Because there was only a 4 mass unit difference between DMPC and (14:1) PC, the isotopic patterns corresponding to [peptide+DMPC] and [peptide+(14:1)PC] complexes exhibited considerable overlap. This made it inconvenient to readily compare the relative binding strengths.

Degree of unsaturation

The hydrophobic interaction should be strengthened as the lipid tail chain length increases. So far, in neat aqueous solution, P294 showed a similar level of affinity to both DLPC and DMPC, P326 showed higher affinity to DLPC than DMPC. As the chain length increased, the stronger hydrophobic interaction could be counterbalanced and even overwhelmed by decreases in the ionization efficiency and/or a decrease in the electrostatic interaction. As mentioned before, the presence of double bonds decreases the

magnitude of the hydrophobic interactions. In terms of hydrophobicity, it is estimated that the effect of introducing 2 double bonds is equivalent to the removal of a CH_2 group[104]. Unsaturation largely increases the ES ionization efficiency of the lipid[126]; moreover, all unsaturated model lipids have very low Tm values (-20 and -60 degree for (18:1) and (18:3) PC, respectively). We believe that the comparison of the lipid-peptide binding as a function of degree of unsaturation offers the opportunity to test the effect of hydrophobicity of the lipid on binding. Relative to the case where -CH_2- groups are removed, this comparison can be made with a diminished uncertainty regarding differences in ionization efficiency, electrostatic interaction, and lipid phase.

The first double bond of the polyunsaturated lipid commonly occurs at carbon 9, with additional double bonds potentially occurring at every third carbon atom[104,135]. The model lipids chosen in this set of experiments are: 1,2-Dioleoyl-sn-Glycero-3-Phosphocholine and 1,2-Dilinolenoyl-sn-Glycero-3-Phosphocholine, simplified as (18:1)PC and (18:3)PC, respectively. In a P294:(18:1):(18:3) = 20:20:20 μM aqueous solution, the [P294+(18:1)PC] and P294+(18:3)PC] complexes exhibited isotope patterns that were totally resolved from one another (Fig. 7). Results indicate that (18:1)PC binds slightly more strongly to P294 than (18:3)PC, yielding binding strengths 0.12 ± 0.01 and 0.09 ± 0.01, respectively. To address the possibility that the binding strength difference may come from an imprecise concentration ratio of (18:1)PC and (18:3)PC, a batch of P294:(18:1):(18:3) = 20:40:40 μM aqueous solution was made (Fig. 7). The binding strength for [P294+(18:1)PC] and [P294+(18:3)PC] complexes were 0.16 ± 0.01 and 0.13 ± 0.01,respectively.

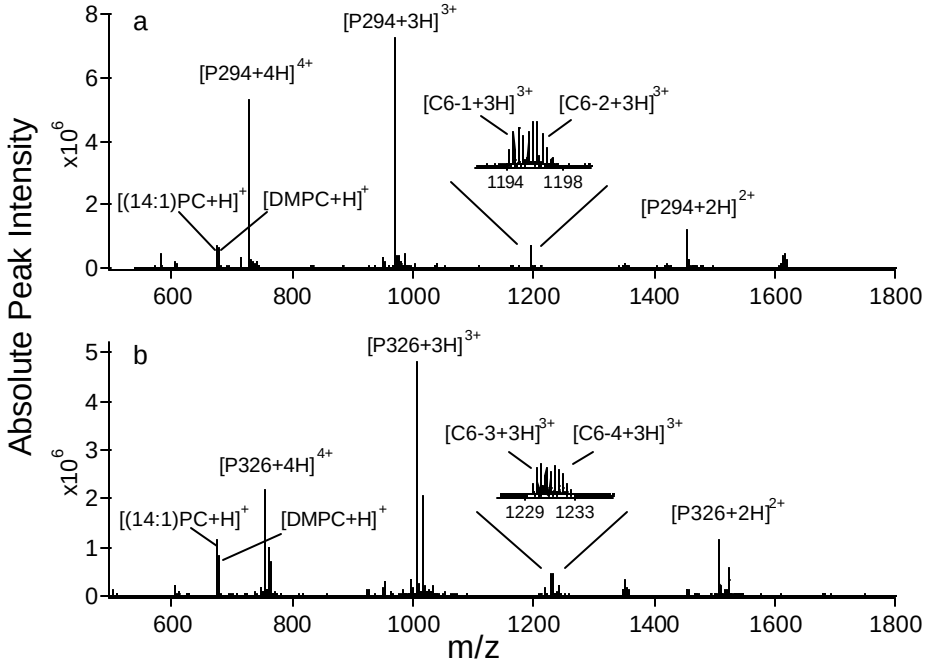

Fig. 6. Electrospray mass spectra of (a) P294:(14:1)PC:DMPC (20:20:20 µM) aqueous solution; and (b) P326:(14:1)PC:DMPC (20:20:20 µM) aqueous solution. Both P294 and P326 showed similar level of affinity to (14:1)PC as to DMPC. In 6a, "C6-1" represents [P294+(14:1)PC] complex; "C6-2" represents [P294+DMPC] complex. In 6b, "C6-3" represents [P326+(14:1)PC] complex; "C6-4" represents [P326+DMPC] complex. The isotopic patterns corresponding to [peptide+DMPC] and [peptide+(14:1)PC] complexes exhibited considerable overlap.

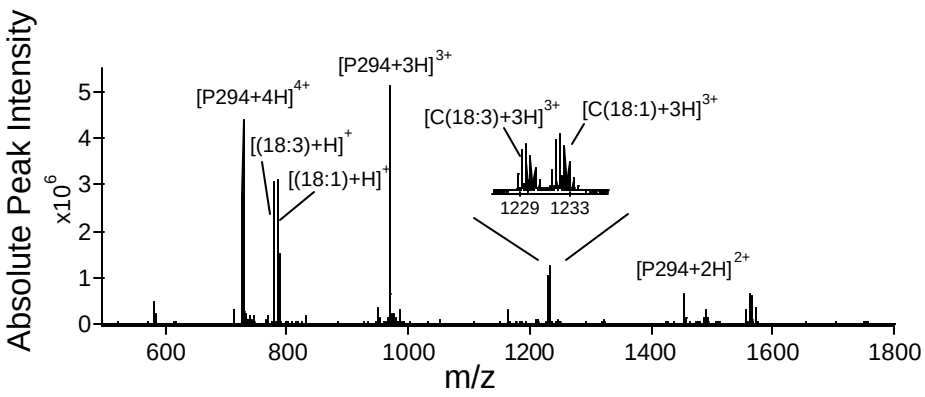

Fig. 7., Electrospray mass spectra of P294:(18:1)PC:(18:3)PC (20:40:40 µM) aqueous solution. “(18:1)” represents (18:1)PC]; “(18:3)” represents (18:3)PC]; “C(18:1)” represents [P294+(18:1)PC] complex; “C(18:3)” represents [P294+(18:3)PC] complex.

Conclusion

Detailed binding specificities between selected phospholipids and model fusion peptides were investigated. Negatively charged DMPG clearly bound more strongly to P294 and P326 than zwitterionic DMPC. The increased electrostatic interaction played a significant role in stabilizing peptide-PG complexes. Binding between P294/P326 and PC/PG in 100% aqueous solution was destroyed by addition of methanol, with a higher percentage of methanol needed to destroy a stronger binding in pure aqueous solution. Further increases in the methanol volume fraction generally resulted in re-appearance of peptide-lipid binding, with binding strengths of DLPC/PG-peptide complexes rising more steeply than DMPC/PG-peptide complexes. These results indicated that detected P294/P326-lipid complexes were already formed in 100% aqueous solution, with the hydrophobic effect being the primary driving force promoting the interaction. The fact that hydrophilic fibrinopeptide B showed much weaker affinity to zwitterionic DMPC than fusion peptide P294 and P326 offered further evidence that hydrophobic interactions in solution were contributing heavily to the formation of [P294/P326+PC] complexes. Fibrinopeptide B had moderate binding affinity to DMPG in 100% aqueous solution. However, upon addition of increasing amount of methanol, it showed only a minor initial decrease in binding to lipids before the detected binding strength eventually increased. This contrasting result offered additional evidence that hydrophobic forces play a key role in the mass spectrometrically observed binding between the fusion peptide and PG.

P326 showed stronger affinity to DMPC than P294 over the entire range, $3.2 < pH < 5.5$. The P326-DMPC binding had an immediate and steeper decrease as pH was lowered,

whereas the P294-DMPC binding was slightly strengthened at pH 3.7 then decreased gradually with a further lowering of pH.

Both P326 and P294 exhibited affinity toward unsaturated lipids. (18:1)PC bound slightly more strongly to P294 than (18:3)PC. The comparison of the lipid-peptide binding as a function of degree of unsaturation offers the opportunity to test the effect of hydrophobicity of the lipid on binding.

These experiments help to establish ES-MS as a viable new biotechnology tool capable of providing valuable information regarding the strength of hydrophobically driven, noncovalent interactions.

REFERENCES

1) Zeleny, J. Phys. Rev. 1917, 10,1-6, 1-6.
2) Bruins, A. P.; Covey, T. R.; Henion, J. D. Anal. Chem. 1987, 59, 2642-2646.
3) Smith, R. D.; Olivares, J. A.; Nguyen, N. T.; Udseth, H. R. Anal. Chem. 1988, 60, 436-441.
4) Covey, T. R.; Bonner, R. F.; Shushan, B. I.; Henion, J. Rapid Commun. Mass Spectrom. 1988, 2, 249-256.
5) Fenn, J. B. M., M.; Meng, C. K.; Wong, S. F.; Whitehouse, C. M. Science 1989, 246, 64-71.
6) Taylor, G. I. Proc. R. Soc. London 1964, A280, 383-397.
7) Pfeifer, R. J.; Hendricks, C. D. AIAA Journal 1968, 6, 496-502.
8) Dole, M.; Mack, L. L.; Hines, R. L.; Mobley, R. C.; Ferguson, L. D.; Alice, M. B. J. Chem. Phys. 1968, 49, 2240-2249.
9) Iribarne, J. V.; Thomson, B. A. J. Chem. Phys. 1976, 64, 2287-2294.
10) Smith, D. P. H. IEEE Trans. Ind. App. 1986, IA-22, 527-535.
11) Hayati, I.; Bailey, A. I.; Tadros, T. F. Nature 1986, 319, 41-43.
12) Hayati, I.; Bailey, A. I.; Tadros, T. F. J. Colloid and Interface Sci. 1987, 117, 205-230.
13) Taflin, D. C.; Ward, T. L.; Davis, E. J. Langmuir 1989, 5, 376-384.
14) Blades, A. T.; Ikonomou, M. G.; Kebarle, P. Anal. Chem. 1991, 63, 2109-2114.
15) Zarin, F.; Kaufman, S. L.; Socha, J. R. J. Aerosol, Sci 1991, 22, Suppl. 1, S343-S346.
16) Ikonomou, M. G.; Blades, A. T.; Kebarle, P. Anal. Chem. 1991, 63, 1989-1998.
17) Cole, R. B.; Harrata, A. K. Rapid Commun. Mass Spectrom. 1992, 6, 536-539.
18) Kebarle, P.; Tang, L. Anal. Chem 1993, 65, 972A-986A.
19) Le Blanc, J. C. Y.; Wang, J.; Guevremont, R.; Siu, K. W. M. Org. Mass. Spectrom. 1994, 29, 587-593.
20) Fernandez de la Mora, J.; Locertales, I. G. J. Fluid Mech. 1994, 243, 561.
21) Van Berkel, G. J.; Zhou, F. Anal. Chem 1995, 67, 2916-2923.
22) Enke, C. G. Anal. Chem. 1997, 69, 4885-4893.
23) Wilm, M.; Mann, M. Anal. Chem. 1996, 68, 1-8.
24) Juraschek, R.; Dulcks, T.; Karas, M. Journal of the American Society for Mass Spectrometry 1999, 10, 300-308.
25) Cole, R. B.; Harrata, A. K. J. Am. Soc. Mass. Spectrom. 1993, 4, 546-556.
26) De la Mora, J. F.; Van Berkel, G. J.; Enke, C. G.; Cole, R. B.; Martinez-Sanchez, M.; Fenn, J. B. Journal of Mass Spectrometry 2000, 35, 939-952.
27) Juhasz, P.; Ikonomou, M. G.; Blades, A. T.; Kebarle, P. NATO ASI Series, Series B: Physics 1991, 269(Methods Mech. Prod. Ions Large Mol.), 171-184.

28) Van Berkel, G. J.; Giles, G. E.; Bullock IV, J. S.; Gray, L. J. Anal. Chem. 1999, 71, 5288-5296.

29) Fenn, J. B. M., M.; Meng, C. K.; Wong, S. F.; Whitehouse, C. M. Science 1989, 246, 64-71.
30) Smith, R. D.; Loo, J. A.; Ogorzalek Loo, R. R.; Busman, M.; Udseth, H. R. Mass Spectrom. Rev. 1991, 10, 359-451.
31) Covey, T. R.; Bonner, R. F.; Shushan, B. I.; Henion, J. Rapid Commun. Mass Spectrom. 1988, 2, 249-256.
32) Chowdhury, S. K.; Katta, V.; Chait, B. T. J. Am. Chem. Soc. 1990, 112, 9012-9013.
33) Loo, A.; Edmonds, C. G.; Udseth, H. R.; Smith, R. D. Anal. Chem. 1990, 62, 693-698.
34) Katta, V.; Chowdhury, S. K.; Chait, B. T. J. Am. Chem. Soc. 1990, 112, 5348-5349.
35) Mirza, U. A.; Cohen, S. L.; Chait, T. Anal. Chem. 1993, 65, 1-6.
36) Fenn, J. B. J. AM. Soc. Mass Spectrom. 1993, 4, 524-535.
37) Dole, M.; Mack, L. L.; Hines, R. L.; Mobley, R. C.; Ferguson, L. D.; Alice, M. B. J. Chem. Phys. 1968, 49, 2240-2249.
38) Iribarne, J. V.; Thomson, B. A. J. Chem. Phys. 1976, 64, 2287-2294.
39) Kebarle, P.; Tang, L. Anal. Chem 1993, 65, 972A-986A.
40) Wang, G.; Cole, R. B. Anal. Chem. 1995, 67, 2892-2900.
41) Enke, C. G. Anal. Chem. 1997, 69, 4885-4893.
42) Le Blanc, J. C. Y.; Beauchemin, D.; Siu, K. W. M.; Guevremont, R.; Berman, S. S. Org. Mass. Spectrom. 1991, 26, 831-839.
43) Downard, K. M.; Biemann, K. Int. J. Mass Spectrom. Ion Process 1995, 148, 191-202.
44) Chowdhury, S. K.; Katta, V.; Chait, B. T. Rapid Commun. Mass Spectrom. 1990, 4, 81-87.
45) Smith, R. D.; Loo, J. A.; Edmonds, C. G.; Barinaga, C. J.; Udseth, H. R. Anal. Chem. 1990, 62, 882-899.
46) Ikonomou, M. G.; Blades, A. T.; Kebarle, P. Anal. Chem. 1990, 62, 957-967.
47) McLuckey, S. A.; Van Berkel, G. J.; Glish, G. L. J. Am. Chem. Soc. 1990, 112, 5668-5670.
48) Smith, R. D.; Loo, J. A.; Barinaga, C. J.; Edmonds, C. G.; Udseth, H. R. J. Am. Soc. Mass Spectrom. 1990, 1, 53-65.
49) McLuckey, S. A.; Glish, G. L.; Van Berkel, G. J. Anal. Chem. 1991, 63, 1971-1978.
50) Winger, B. E.; Light-Wahl, K. J.; Smith, R. D. J. Am. Soc. Mass Spectrom. 1992, 3, 624-630.
51) Ogorzalek Loo, R. R.; Loo, J. A.; Udseth, H. R.; Fulton, J. L.; Smith, R. D. Rapid Commun. Mass Spectrom. 1992, 6, 159-165.
52) Cassady, C. J.; Wronka, J.; Kruppa, G. H.; Laukien, F. H. Rapid Commun. Mass Spectrom. 1994, 8, 394-400.
53) Le Blanc, J. C. Y.; Wang, J.; Guevremont, R.; Siu, K. W. M. Org. Mass. Spectrom. 1994, 29, 587-593.

54) Gronert, S. Journal of Mass Spectrometry 1999, 34, 787-796.
55) Amad, M. H.; Cech, N. B.; Jackson, G. S.; Enke, C. G. J. Mass Spectrom. 2000, 35, 784-789.
56) Loo, J. A.; Udseth, H. R.; Smith, R. D. Rapid Comm. Mass Spectrom. 1988, 2, 207-210.
57) Guevremont, R.; Siu, K. W. M.; LeBlanc, J. C. Y.; Berman, S. S. J. Am. Soc. Mass Spectrom. 1992, 3, 216-224.
58) Kelly, M. A.; Vestling, M. M.; Fenselau, C. C.; Smith, P. B. Org. Mass Spectrom. 1992, 27, 1143-1147.
59) Wang, G.; Cole, R. B. Org. Mass. Spectrom. 1994, 29, 419-427.
60) Konermann, L. S., Eloi A.; Sogbein, Olusola F. Analytical Chemistry 2001, 73, 4836-4844.
61) Cole, R. B.; Harrata, A. K. Rapid Commun. Mass Spectrom. 1992, 6, 536-539.
62) Cole, R. B.; Harrata, A. K. J. Am. Soc. Mass. Spectrom. 1993, 4, 546-556.
63) Wang, G.; Cole, R. B. Anal. Chem. 1994, 66, 3702-3708.
64) Ashton, D. S.; Beddell, C. R.; Cooper, D. J.; Green, B. N.; Oliver, R. W. A. Org. Mass Spectrom. 1993, 28, 721-728.
65) Schmidt, A.; Bahr, U.; Karas, M. Anal. Chem. 2001, 73, 6040-6046.
66) Wilm, M.; Mann, M. Anal. Chem. 1996, 68, 1-8.
67) Wilm, M.; Mann, M. Int. J. Mass Spectrom. 1994, 136, 167-180.
68) Juraschek, R.; Dulcks, T.; Karas, M. Journal of the American Society for Mass Spectrometry 1999, 10, 300-308.
69) Karas, M.; Bahr, U.; Dulcks, T. Fresenius' Journal of Analytical Chemistry 2000, 366.
70) Murphy III, J. P.; Valaskovic, G. A. 2002 ASMS Meeting, Orlando, FL 2002.
71) Busman, M.; Rockwood, A. L.; Smith, R. D. Journal of Physical Chemistry 1992, 96, 2397-2400.
72) Thomson, B. A. Journal of the American Society for Mass Spectrometry 1997, 8, 1053-1058.
73) Van Den Bremer, E. T. J.; Jiskoot, W.; James, R.; Moore, G. R.; Kleanthous, C.; Heck, A. J. R.; Maier, C. S. Protein Science 2002, 11, 1738-1752.
74) Comisarow, M. B.; Marshall, A. G. Chem. Phys. Lett. 1974a, 25, 282-283
75) Loo, J. A.; Quinn, J. P.; Ryu, S. I.; Henry, K. D.; Senko, M. W. McLafferty, F. W. Proc. Natl. Acad. Sci. USA 1992, 89, 286.
76) Winger, B. E.; Hofstadler, S. A.; Bruce, J. E.; Udseth, H. R.; Smith, R. D. J. Am. Soc. Mass Spectrom. 1993, 4, 566.
77) Koster, C.; Castoro, J. A.; Wilkins, C. L. J. Am. Chem. Soc. 1992, 114, 7572.
78) Li, Y. Z.; Little, D. P.; Koster, H.; Hunter, R. L.; Mclver, R. T. Jr, Anal. Chem. 1996, 68, 2090.
79) Drummond, J. T.; Ogorzalek Loo, R. R.; Matthews, R. G. Biochemistry 1993, 32, 9282-9289.
80) Ganem, B.; Li, Y.-T.; Henion, J. D. J. Am. Chem. Soc. 1991, 113, 7818-7819
81) Cheng, X. H.; Harms, A. C.; Goudreau, P. N.; Tetwilliger, T. C.; Smith, R. D. Proc. Natl. Acad. Sci. USA 1996, 93, 7022-7027.
82) Greig, M. J.; Gaus, H.; Cummins, L. L.; Sasmor, H.; Griffey, R. H. J. Am. Chem. Soc. 1995, 117, 10765-10766.

83) Eckert, D. M.; Kim, P. S. Annual Review of Biochemistry 2001, 70, 777-810.
84) Peisajovich, S. G.; Shai, Y. Trends in Biochemical Sciences 2002, 27, 183-190.
85) Epand, R. M. Biochimica et Biophysica Acta 2003, 1614, 116-121.
86) Voglino, L.; McIntosh, T. J.; Simon, S. A. Biochemistry 1998, 37, 12241-12252.
87) Jacobs, R. E.; White, S. H. Biochemistry 1989, 28, 3421-37.
88) Jones, J. D.; Gierasch, L. M. Biophysical Journal 1994, 67, 1546-61.
89) Ben-Shaul, A.; Ben-Tal, N.; Honig, B. Biophysical Journal 1996, 71, 130-137.
90) Morris, M. C.; Chaloin, L.; Heitz, F.; Divita, G. Curr Opin Biotechnol 2000, 11, 461-466.
91) Ganem, B.; Li, Y. T.; Henion, J. D. Journal of the American Chemical Society 1991, 113, 7818-19.
92) Katta, V.; Chait, B. T. Journal of the American Chemical Society 1991, 113, 8534-5.
93) Daniel, J. M.; Friess, S. D.; Rajagopalan, S.; Wendt, S.; Zenobi, R. International Journal of Mass Spectrometry 2002, 216, 1-27.
94) Light-Wahl, K. J.; Winger, B. E.; Smith, R. D. Journal of the American Chemical Society 1993, 115, 5869-70.
95) Loo, R. R. O.; Goodlett, D. R.; Smith, R. D.; Loo, J. A. Journal of the American Chemical Society 1993, 115, 4391-2.
96) Knight, W. B.; Swiderek, K. M.; Sakuma, T.; Calaycay, J.; Shively, J. E.; Lee, T. D.; Covey, T. R.; Shushan, B.; Green, B. G.; Chabin, R.; Shah, S.; Mumford, R.; Dickinson, T. A.; Griffin, P. R. Biochemistry 1993, 32, 2031-5.
97) Fitzgerald, M. C.; Chernushevich, I.; Standing, K. G.; Whitman, C. P.; Kent, S. B. H. Proceedings of the National Academy of Sciences of the United States of America 1996, 93, 6851-6856.
98) Huang, H. W.; Wang, K. T. Biochemical and Biophysical Research Communications 1996, 227, 615-21.
99) Demmers, J. A. A.; van Dalen, A.; de Kruijff, B.; Heck, A. J. R.; Killian, J. A. FEBS Letters 2003, 541, 28-32.
100) de Brouwer, A. P. M.; Versluis, C.; Westerman, J.; Roelofsen, B.; Heck, A. J. R.; Wirtz, K. W. A. Biochem. 2002, 41, 8013-8018.
101) Li, Y.; Heitz;, F.; Grimellec;, C. L.; Cole, R. B. Proceedings of the 51st ASMS Conference on Mass Spectrometry and Allied Topics, Montreal, Canada, June 9, 2003 .
102) Li, Y.; Heitz;, F.; Grimellec;, C. L.; Cole, R. B. Rapid Commun. Mass Spectrom. in press.
103) Hearn, M. T. W.; Zhao, G. Analytical Chemistry 1999, 71, 4874-4885.
104) Tanford, C. The hydrophobic Effect: Formation of Micelles and Biological Membranes 1980.
105) Xu, X.; Lu, W.; Cole, R. B. Anal. Chem. 1996, 68, 4244-4253.
106) Lu, W.; Xu, X.; Cole, R. B. Anal. Chem. 1997, 69, 2478-2484.
107) Van Berkel, G. J. Journal of Mass Spectrometry 2000, 35, 773-783.
108) Van Berkel, G. J.; Zhou, F.; Aronson, J. T. Int J. Mass Spectrom. & Ion Process. 1997, 162, 55-67.
109) Cloupeau, M.; Prunet-Foch, B. Journal of Aerosol Science 1994, 25, 1021-1036.
110) Tang, L.; Kebarle, P. Anal. Chem. 1993, 65, 3654-3668.

111) Wang, G.; Cole, R. B. Anal. Chem. 1994, 66, 3702-3708.
112) Zhou, F.; Van Berkel, G. J. Anal. Chem. 1995, 67, 3643-3649.
113) Tang, L.; Kebarle, P. Anal. Chem. 1991, 63, 2709-2715.
114) Billon, J. P. Journal of Electroanalytical Chemistry 1959/60, 1, 486-501.
115) Kebarle, P.; Ho, Y. In Electrospray Ionization Mass Spectrometry: Fundamentals, Instrumentation & Applications; John Wiley & Sons, I., Ed.; Cole, R. B.: NY, 1997, pp 3-63.
116) Pfeifer, R. J.; Hendricks, C. D. AIAA Journal 1968, 6, 496-502.
117) Mussini, T.; Covington, A. K.; Dal Pozzo, F.; Longhi, P.; Rondinini, S.; Zou, Z.-Y. 1983, 28, 1593-1598.
118) Van Berkel, G. J.; Zhou, F.; Aronson, J. T. Int J. Mass Spectrom. & Ion Process. 1997, 162, 55-67.
119) Fernandez de la Mora, J.; Locertales, I. G. J. Fluid Mech. 1994, 243, 561.
120) Personal communication with New Objective.
121) Schnier, P. D.; Gross, D. S.; Williams, E. R. J. Am. Chem. Soc. 1995, 117, 6747.
122) Cohen, F. S.; Melikyan, G. B. Nature Structural Biology 2001, *8*, 653-655.
123) Reynolds, J. A.; Tanford, C.; Stone, W. L. Proceedings of the National Academy of Sciences of the United States of America 1977, 74, 3796-3799.
124) Smith, R.; Tanford, C. Journal of Molecular Biology 1972, 67, 75-83.
125) King, M. D.; Marsh, D. Biochemistry 1987, 26, 1224-1231.
126) Koivusalo, M.; Haimi, P.; Heikinheimo, L.; Kostiainen, R.; Somerharju, P. Journal of Lipid Research 2001, 42, 663-672.
127) Kofeler, H. C.; Rechberger, G. N.; Fauler, G.; Windischhofer, W.; Leis, H.-J. Proceedings of the 51st ASMS Conference on Mass Spectrometry and Allied Topics, Montreal, Canada, June 9, 2003 2003.
128) Lewis, R. N. A. H.; Prenner, E. J.; Kondejewski, L. H.; Flach, C. R.; Mendelsohn, R.; Hodges, R. S.; McElhaney, R. N. Biochemistry 1999, 38, 15193-15203.
129) Turchiello, R. F.; Juliano, L.; Ito, A. S.; Lamy-Freund, M. T. Biopolymers 2000, 54, 211-221.
130) Pedersen, T. B.; Sabra, M. C.; Frokjaer, S.; Mouritsen, O. G.; Jorgensen, K. Chemistry and Physics of Lipids 2001, 113, 83-95.
131) Tomczak, M. M.; Hincha, D. K.; Crowe, J. H.; Harding, M. M.; Haymet, A. D. J. FEBS Letters 2003, 551, 13-19.
132) Brandenburg, K.; Harris, F.; Dennison, S.; Seydel, U.; Phoenix, D. European Journal of Biochemistry 2002, 269, 5414-5422.
133) Morein, S.; Killian, J. A.; Sperotto, M. M. Biophysical Journal 2002, 82, 1405-1417.
103) Hearn, M. T. W.; Zhao, G. Analytical Chemistry 1999, 71, 4874-4885.
134) Pritsker, M.; Rucker, J.; Hoffman, T. L.; Doms, R. W.; Shai, Y. Biochemistry 1999, 38, 11359-11371.
135) Voet, D.; Voet, J. G.; Pratt, C. John Wiley & Sons, Inc.

APPENDIX

Appendix A

The purpose of this calculation is to rationalize the observation that #1 μm tips can give slightly larger ES currents than those of #2 μm tips.

$E = 2V_c \times [r_c \ln(4d/r_c)]^{-1}$, while $d = 3 * 10^{-3}$ m, V_c is the high voltage applied, r_c is the outer radius of the tip.

	#1 μm tip	#2 μm tip	#5 μm tip
OD [m]	$1.4x10^{-6}$	$3.5x10^{-6}$	$5.6x10^{-6}$
$\mathbf{r_c}$ [m]	$0.7x10^{-6}$	$1.8x10^{-6}$	$2.8x10^{-6}$
$\mathbf{[r_c \ln(4d/r_c)]^{-1}}$	$1.5x10^{5}$	$0.63x10^{5}$	$0.43x10^{5}$
E[V/m]	$3.0\ V_c x10^{5}$	$1.3\ V_c x10^{5}$	$0.86\ V_c\ x10^{5}$

$ESC = [(4\pi/\varepsilon)^3 (9\gamma)^2 \varepsilon_o{}^5]^{1/7} (KE)^{3/7} (V_f)^{4/7}$

If the constant terms are set equal to k, such that $k = [(4\pi/\varepsilon)^3 (9\gamma)^2 \varepsilon_o{}^5]^{1/7} (K)^{3/7}$, then the the equation reduces to $ESC = k\,(E)^{3/7} (V_f)^{4/7}$

	#1 μm tip	#2 μm tip	#5 μm tip
$\mathbf{V_f}$ [L /sec]	$1.3x10^{-9}$	$2.0x10^{-9}$	$5.3x10^{-9}$
$\mathbf{(V_f)^{4/7}}$	$8.36x10^{-6}$	$10.7x10^{-6}$	$18.7x10^{-6}$
E [V/m]	$3.0\ V_c x10^{5}$	$1.3\ V_c x10^{5}$	$0.86\ V_c x10^{5}$
$\mathbf{(E)^{3/7}}$	$2.23x10^{2}x(V_c)^{3/7}$	$1.55x10^{2}x(V_c)^{3/7}$	$1.30x10^{2}x(V_c)^{3/7}$
I [A]	$1.9x10^{-3}x(V_c)^{3/7}xk$	$1.7x10^{-3}x(V_c)^{3/7}xk$	$2.4x10^{-3}x(V_c)^{3/7}xk$

Thus, compared to the #2 μm tip, ES current can be larger for the #1 μm tip due primarily to the increased field strength (E).

Appendix B

Typical values of N/N_0 are calculated below for the three employed spray tips using a fixed ES current.

$N/N_0 = (I / e) / (ACV_f)$

$A = 6.023 \times 10^{23}$; $C = 20 \times 10^{-6}$ mol/L;

When I = 10 nA, $I/e = 10 \times 10^{-9} / (1.602 \times 10^{-19}) = 6.242 \times 10^{10}$;

The measured V_f values for #1 μm, #2 μm, and #5 μm tip are 1.3×10^{-9}, 2.0×10^{-9}, and 5.3×10^{-9} L/sec, respectively. Substituting these numbers into the equation above, the N/N_0 for #1 μm, #2 μm, and #5 μm tips are calculated to be 4.0, 2.6, and 1.0, respectively.

VITA

Yan Li got her B.S. and M.S. in Chemistry in 1991 and 1994, respectively, from Nankai University. From 1994 to 1999, she worked at Beijing Research Institute of Chemical Industry as an analytical scientist. Driven by intrinsic needs for new experience, she came to University of New Orleans to pursue a Ph.D. in Analytical Chemistry in 1999.